



Swiss Federal Institute of Technology Zurich

Seminar for  
Statistics

Department of Mathematics

---

Master Thesis

Spring 2022

---

Lukas Graz

**Interpolation and Correction  
of  
Multispectral Satellite Image Time Series**

---

Submission Date: September 18th, 2022

---

Co-Adviser: Gregor Perich  
Adviser: Prof. Dr. Nicolai Meinshausen



# Preface

## Supplementary Material

Instructions and the relevant code needed to reproduce this thesis can be found in the [GitHub repository](#) and to use our results we recommend the provided [R-package](#).

More information is given in the appendix [A](#).

## Acknowledgements

First, I wish to express my sincere gratitude to my supervisor Prof. Dr. Nicolai Meinshausen who took the responsibility for my work and happily took the time to discuss conceptual and guiding questions, and to inspire me with new ideas.

This endeavor would not have been possible without Gregor Perich. His high personal commitment, reliability as well as the weekly instructive supervision meetings were essential for this work.

It was a real pleasure for me to be part of the *Crop Science* group for this time. Enjoying everyday company, a two-day excursion, and harvesting wheat together made this time truly remarkable. In particular, I would like to thank Prof. Dr. Achim Walter, who supported this collaboration at its core.

Last but not least, I would like to express my gratitude to the *Seminar for Statistics*, which created the framework conditions for this work and did everything to help me with conceptional and administrative questions. I should also mention the computing resources provided by them, without which my computations would not have been feasible.



# Abstract

Multispectral satellite imagery is used to model vegetation characteristics and development on a large scale in agriculture. As an example, satellite-derived Time Series (TS) of spectral indices like the Normalized Difference Vegetation Index (NDVI) are used to classify crops and to predict crop yield. Sometimes satellite measurements do not match the ground signal due to contamination by clouds and other atmospheric effects. Therefore, traditional approaches aim to filter out contaminated observations before extracting and subsequently interpolating the NDVI. After filtering, remaining contaminated observations and resulting data gaps are the two challenges for interpolation that we address in this thesis. For this purpose, cereal crop yield maps from 2017-2021 of a farm in Switzerland with the corresponding Sentinel 2 satellite image TS published by the European Space Agency were examined. Contaminated observations were filtered with the provided Scene Classification Layer (SCL). We give a benchmark-supported review of different interpolation methods. Based on it, we found Smoothing Splines as a flexible non-parametric method and Double Logistic approximation as a parametric method with implicit shape assumptions to perform most favorably given the aforementioned challenges. In addition, we generalize an iterative technique which robustifies interpolation methods against outliers by reducing their weights. In most cases, this robustification successfully decreased the 50% and 75% quantiles of the absolute out-of-bag residuals. Moreover, we present a general interpolation procedure that utilizes additional information to correct the target variable with an uncertainty estimate and then performs a weighted interpolation. In our setting, the target variable is the NDVI and as additional information we use the SCL, the observed NDVI and the spectral bands. Consequently, we no longer filter using the SCL, but weight observations according to their reliability. Applying this procedure, the unexplained variance in crop yield estimations via the resulting NDVI TS decreased by 10.5%. Considering the success of the presented procedure with respect to NDVI TS, it appears promising for applications to other satellite-based TS given its cloud-correcting properties.

## Contents

<b>Notation</b>	<b>xi</b>
<b>1 Introduction</b>	<b>1</b>
<b>2 Data and Methods</b>	<b>3</b>
2.1 Sentinel 2 Data . . . . .	3
2.2 Crop Yield Data . . . . .	3
2.3 Normalized Difference Vegetation Index . . . . .	4
2.4 Transformation of Timescale . . . . .	5
2.5 The Concept of a ‘Pixel’ . . . . .	6
2.6 Illustration of S2 Images . . . . .	6
2.7 Estimation Evaluation Criteria . . . . .	6
2.7.1 Score Functions . . . . .	6
2.7.2 Out-Of-Bag and Leave-One-Out-Cross-Validation . . . . .	8
<b>3 Interpolation</b>	<b>9</b>
3.1 Interpolation Setup . . . . .	9
3.2 Parametric Regression . . . . .	9
3.2.1 Double Logistic . . . . .	10
3.2.2 Fourier Series . . . . .	10
3.2.3 Optimization Issues . . . . .	11
3.3 Non-Parametric Regression . . . . .	11
3.3.1 Kernel Regression: Nadaraya-Watson . . . . .	11
3.3.2 Universal Kriging . . . . .	12
3.3.3 Savitzky-Golay Filter . . . . .	13
3.3.4 Locally Weighted Regression . . . . .	15
3.3.5 B-Splines . . . . .	16
3.3.6 Smoothing Splines . . . . .	16
3.4 Tuning Parameter Estimation . . . . .	17
3.5 Robustification . . . . .	17
3.5.1 Our Adjustment: . . . . .	18
3.5.2 Examples and Conclusions . . . . .	19
3.5.3 Upper Envelope Approach . . . . .	19
3.6 Performance Assessment . . . . .	19
<b>4 NDVI Correction</b>	<b>23</b>
4.1 Considering other SCL Classes . . . . .	23
4.2 Correction Models . . . . .	24
4.2.1 Ordinary Least Squares . . . . .	24
4.2.2 Least Absolute Shrinkage and Selection Operator . . . . .	25
4.2.3 General Additive Model . . . . .	26
4.2.4 Random Forest . . . . .	26
4.2.5 Multivariate Adaptive Regression Splines . . . . .	27
4.3 Weighted Interpolation . . . . .	28
4.4 Resulting Interpolation Strategies . . . . .	28
4.5 Evaluation via (relative) Yield Prediction Error . . . . .	29

<b>5 Results</b>	<b>33</b>
5.1 Goodness of Fit for Selected IMs . . . . .	33
5.2 Yield Prediction Error for Tested ISs . . . . .	33
<b>6 Discussion</b>	<b>35</b>
6.1 Interpolation . . . . .	35
6.1.1 Score Functions . . . . .	35
6.1.2 Data Gaps in Time Series . . . . .	35
6.1.3 Preselection . . . . .	36
6.1.4 Candidate Selection . . . . .	36
6.2 NDVI Correction . . . . .	37
6.2.1 Using Additional Covariates . . . . .	37
6.2.2 IS Selection . . . . .	37
6.2.3 Error Sources in Yield Estimation . . . . .	37
6.2.4 NDVI Correction as Unsupervised Learning . . . . .	38
<b>7 Conclusion</b>	<b>39</b>
7.1 Future Work . . . . .	40
7.1.1 Time Series Correction-Interpolation as a General Method . . . . .	40
7.1.2 Minor Improvements . . . . .	41
<b>Bibliography</b>	<b>43</b>
<b>A Reproducibility</b>	<b>47</b>
A.1 Reproduce Results . . . . .	47
A.2 R-Package . . . . .	47
<b>B Further Material</b>	<b>49</b>
B.1 Data and Methods . . . . .	49
B.1.1 NDVI . . . . .	49
B.1.2 GDD . . . . .	49
B.2 Interpolation . . . . .	50
B.2.1 Parameter Bounds . . . . .	50
B.2.2 Iterations for Robustification . . . . .	50
B.3 NDVI correction . . . . .	52
B.3.1 OLS <sup>SCL</sup> Model Outputs . . . . .	53

**List of Figures**

2.1	Crop yield density map of a field . . . . .	5
2.2	NDVI TS plotted against DAS and GDD . . . . .	5
2.3	Satellite images of a field at selected times + NDVI TS . . . . .	7
3.1	Fourier approximation and Double Logistic . . . . .	11
3.2	Gaussian Variogram . . . . .	13
3.3	Effect of variogram parameters and failure of maximum likelihood. . . . .	13
3.4	Smoothing splines optimized by minimizing the given quantile of the absolute leave-one-out residuals . . . . .	18
3.5	Smoothing splines robustification. . . . .	19
3.6	The LOESS smoother robustification. . . . .	20
4.1	Smoothing splines fit considering SCL45. . . . .	23
4.2	'True' vs. observed NDVI — for each SCL class . . . . .	31
B.1	Spectral reflectance of the green/dry vegetation . . . . .	49
B.2	B-splines robustification. . . . .	50
B.3	A Double Logistic curve robustification. . . . .	51
B.4	Stepwise illustration of robust NDVI correction. . . . .	52

**List of Tables**

2.1	List of spectral bands of the S2-satellites. . . . .	4
2.2	Overview: Scene Classification Layers (SCL) . . . . .	4
3.1	Overview of the studied interpolation methods. . . . .	21
5.1	Goodness of fit for IMs measured with score functions. . . . .	33
5.2	relative RMSE for yield prediction in t/ha . . . . .	34
B.1	RMSE for yield prediction in t/ha . . . . .	52
B.2	Coefficient of determination of yield prediction . . . . .	53



# Notations

Since this thesis, despite its applied nature, is located at the Mathematics Department, we adhere to the convention of speaking in the first-person plural ‘we’. Furthermore, only equations that are referenced elsewhere are equipped with a number.

## Variables

$\lambda \in \mathbb{R}$	A scalar.
$n \in \mathbb{N}$	Sample size.
$i, j$	Indices in $\{1, \dots, n\}$ .
$t \in \mathbb{R}^n$	Time — usually in GDD.
$v \in \mathbb{R}^n$	Absolute residuals of $\widehat{\text{NDVI}}^{\text{true}}$ (see. equation 4.3.0.1)
$w \in \mathbb{R}^n$	Vector of weights for each location $x$ .
$y \in \mathbb{R}^n$	Response in 1-dim interpolation setting.
$\hat{y} \in \mathbb{R}^n$	Estimate of $y$ .
$\bar{y} \in \mathbb{R}$	Sample mean of $y$ .
$r \in \mathbb{R}^n$	Residuals given by $y - \hat{y}$ .
$X \in \mathbb{R}^{n \times p}$	Design matrix. Each row corresponds to one observation and each column to one covariate.
$X_{[:,j]}$	j <sup>th</sup> column of $X$ .
$X_{[i,:]}$	i <sup>th</sup> row of $X$ .

## Abbreviations and Objects

DAS	Days After Sowing.
GDD	Growing Degree Days – cumulative sum of temperature (see. section 2.4).
IM	Interpolation Method. That is a method that interpolates data $(t_i, y_i)_{i=1,\dots,n}$ and returns a function $f(t) = y$ , approximating the data.
IS	Interpolation Strategy. By combining various correction models with different IMs (with and without robustification) in section 4.4 28 ISs were obtained.
LOOCV	Leave One Out Cross Validation. Describes the procedure of estimating the value for a point by a model that has seen all the points except the current one (see section 2.7.2).

NDVI	Normalized Difference Vegetation Index ( <a href="#">Rouse, 1974</a> ). NDVI <sub>true</sub> is the NDVI optained via assumption <a href="#">4.1.0.1</a> and $\widehat{\text{NDVI}}_{\text{true}}$ its estimator introduced in section <a href="#">4.3</a> .
OOB	Out Of the Box. Describes the procedure of estimating the value for a point by a model that has not seen this point before (see section <a href="#">2.7.2</a> ).
Pixel	A data structure that originates from an image pixel and describes a square of $10 \times 10$ meters in the field that coincides with the resolution (and location) of the Sentinel-2 pixels (see. section <a href="#">2.5</a> ). Such pixels are illustrated in figure <a href="#">2.1b</a> .
$P_t$	The observed data (weather and spectral bands) at time $t$ and the location of one pixel.
$P$	A pixel. We see it as a collection of all the $P_t$ at the specified location within one season.
QAR <sup>x</sup>	x% Quantile of Absolute Residuals (see definition <a href="#">2.7.1.2</a> ).
RMSE	Root Mean Square Error (see definition <a href="#">2.7.1.1</a> ).
S2	Sentinel 2 satellites. Two multi-spectral image satellites deployed by the European Space Agency.
SCL	Scene Classification Layer provided by the European Space Agency that gives an estimation of the land cover class of each pixel. It indicates what one can expect at a pixel at a sampled time. For an overview, see table <a href="#">2.2</a> .
TS	Time Series.
YPE	(Relative) Yield Prediction Error (see definition <a href="#">4.5.0.1</a> ).

## Statistical Models

BS	B-splines (see section <a href="#">3.3.5</a> ).
DL	Double Logistic (see section <a href="#">3.2.1</a> ).
FS	Fourier Series (see section <a href="#">3.2.2</a> ).
GAM	General Additive Model (see section <a href="#">4.2.3</a> ).
LASSO	Least Absolute Shrinkage and Selection Operator (see section <a href="#">4.2.2</a> ).
LOESS	Locally Weighted Regression (see section <a href="#">3.3.4</a> ).
MARS	Multivariate Adaptive Regression Splines (see section <a href="#">4.2.5</a> ).
NW	Nadaraya-Watson (see section <a href="#">3.3.1</a> ).
OLS	Ordinary Least Squares (see section <a href="#">4.2.1</a> ).
OLSS <sup>SCL</sup>	OLS using only the observed NDVI and SCL classes (as factor variables).
OLS <sup>all</sup>	OLS using the covariates OLS <sup>SCL</sup> uses and the spectral bands.
RF	Random Forest (see section <a href="#">4.2.4</a> ).
SG	Savitzky-Golay Filter (see section <a href="#">3.3.3</a> ).
SS	Smoothing Splines (see section <a href="#">3.3.6</a> ).
UK	Universal Kriging (see section <a href="#">3.3.2</a> ).

# Chapter 1

## Introduction

Remote sensing aims to measure target variables efficiently from a distance. Large scale monitoring of forest and agricultural vegetation dynamics is of great interest to authorities, insurance companies and research. Examples include crop classification for subsidizing farmers ([Henits et al., 2022](#)) and the creation of crop models for estimating crop yields or nitrogen concentrations ([Courault et al., 2021; Perich et al., 2021](#)). For this, freely distributed multi-spectral satellite imagery from the Sentinel-2 (S2) satellites are examined ([ESA, 2022b](#)). In order to transform the high dimensional satellite images into easily interpretable metrics, spectral indices such as the Normalized Difference Vegetation Index (NDVI) are used ([Rouse, 1974](#)). The NDVI serves as a proxy for photosynthetic activity ([Gamon et al., 1995](#)), and thus the corresponding NDVI Time Series (TS) reflects the vegetation development. The quality of a satellite image, however, depends on atmospheric conditions. Thus, in case of a dense cloud cover, the information content derived from the NDVI is impaired. Therefore, [ESA \(2022a\)](#) also provides a Scene Classification Layer (SCL), which provides additional metadata about what is observed (e.g., shadows, clouds, vegetation, etc.) . So when extracting the NDVI TS from the Sentinel 2 satellite imagery TS, we can filter out the contaminated observations using the SCL classification. However, due to this filtration it may occur that we have no observations for several weeks, especially in winter. It is also possible that some observations are wrongly classified by the SCL (e.g., as vegetation) and thus result in an outlier in the NDVI TS. Consequently, the main challenge is to interpolate an NDVI TS, which can contain large data gaps and outliers.

Currently, there are several approaches to address these issues. One is to look at the observed evolution of the canopy coverage and assume its bell shape for the NDVI TS given the strong correlation between NDVI and photosynthetic activity. Approaches to model this include a 2<sup>nd</sup> order Fourier approximation ([Stöckli and Vidale, 2004](#)) or a Double Logistic function ([Beck et al., 2006](#)). On the other hand, assumptions are made about more abstract properties of the curve, such as smoothness. We divide these into local and global approaches. Nadaraya-Watson ([Strbac et al., 2017](#)), Savitzky-Golay Filter ([Chen et al., 2004](#)) and Locally Reweighted Regression ([Omori et al., 2021](#)) use a sliding window to interpolate the TS stepwise. Global methods like B-Splines ([Gurung et al., 2009](#)) and Smoothing Splines ([Cai et al., 2017a](#)) reduce the squares of all residuals simultaneously, and Universal Kriging fits a Gaussian process to the data ([Chandola and Vatsavai, 2010](#)).

The research questions pursued in this thesis are:

- i.) What are strengths and weaknesses of IMs used in the context of NDVI TS?
- ii.) How may contaminated data be dealt with?
- iii.) How do data gaps affect interpolation?
- iv.) How to deal with data gaps?
- v.) How to assess the quality of an NDVI TS interpolation?

In this thesis, we will discuss the strengths and weaknesses of Interpolation Methods (IMs) and evaluate them with respect to NDVI interpolation. For this purpose, we use the Sentinel 2 satellite image TS and crop yield maps of different fields of different cereal species on a farm in Witzwil, Switzerland over the years 2017-2021. After presenting the available data, illustrating challenges and defining different concepts in chapter 2 (Data and Methods), we turn to the two main blocks of this thesis. One covers the study of IMs and the other presents a general procedure of correcting (NDVI) TS with uncertainty estimation by utilizing additional information. On the first block, in chapter 3 (Interpolation) we examine parametric and non-parametric IMs and discuss their strengths and weaknesses (question i.). We generalize and test an iterative technique that makes IMs more robust to outliers by weighting them less (question ii.). To evaluate IMs, we present an robust approach that uses out-of-bag residuals (question v.). In section 6.1.2 (Data Gaps in Time Series), we discuss how different IMs respond to data gaps (question iii.), and in section 6.1.3 (Preselection) we preselect IMs. This preselection, we evaluate in the results section 5.1 (Goodness of Fit for Selected IMs) and select two candidates from the IMs in section 6.1.4 (Candidate Selection). For the second block, we correct possibly contaminated data with statistical models in chapter 4 (NDVI Correction) (question ii.). Furthermore, we utilize previously ignored observations, which further reduces data gaps (question iv.). Thus, we no longer filter the observations a priori via the SCL, but instead correct the observed NDVI and weight the observations via estimated uncertainties. By combining different statistical models and IMs, we obtain 28 Interpolation Strategies (ISs). We compare those with a vegetation-oriented quality measure (question v.) and describe the results in section 5.2 (Yield Prediction Error for Tested ISs). Based on these results, in section 6.2 (NDVI Correction) we argue what the best IS is. In addition, we justify why our NDVI correction can be understood as unsupervised learning and why we relied only on satellite imagery and not on meteorological data for the NDVI correction. Our conclusions of this thesis, recommendations, as well as an outlook on future work is given in chapter 7 (Conclusion).

# Chapter 2

## Data and Methods

This section describes the available data and the challenges associated with it. Our study region is a farm of over 800ha, which is located in western Switzerland. From [Perich et al. \(2022\)](#) we acquired Sentinel-2 (S2) satellite image data (section [2.1](#)), yield maps of several cereals from 2017 to 2021 (section [2.2](#)), and meteorological data (section [2.5](#)). Methods to evaluate an estimator or model are given in section [2.7](#).

### 2.1 Sentinel 2 Data

The European Space Agency ([ESA, 2022b](#)) freely distributes images of the S2 satellites. Together, both satellites have a revisit time of 5 days in our study region. The S2 images contain 12 spectral bands with spatial resolutions of up to 10 meters (see table [2.1](#)). Bands with a lower resolution (20 and 60 meters) were upscaled to 10 meter resolution using cubic interpolation ([Perich et al., 2022](#)). In order to decrease the effect of atmospheric conditions like reflections and scattering, bottom-of-atmosphere, radiometric corrected Level-2A data was used ([ESA, 2022a](#)). [ESA \(2022a\)](#) also supplies the Scene Classification Layer (SCL). It is a model output that for each location assigns the observed pixel to one of 11 SCL-classes (cf. table [2.2](#)). In this thesis, we will use this classification to filter out data points that we assume to be less informative. These are all observations for which the SCL-class does not correspond to vegetation or bare soils (classes 4 and 5). We define the set SCL45 as the observations that are labelled as SCL-class 4 or 5.

### 2.2 Crop Yield Data

The crop yield data were collected from a combine harvester. Equipped with a satellite-based navigation system, the harvester drives over the fields and continuously estimates the dry crop yield density in  $t/ha$  (cf. figure [2.1a](#)). We use the data set presented in [Perich et al. \(2022\)](#), where error-prone measurement points (such as during a tight curve of the combine harvester) were removed and then the yield maps were rasterized using linear interpolation (cf. figure [2.1b](#)). We summarize the rasterized dry yield values by the following statistics:

Minimum	1st Quartile	Median	Mean	3rd Quartile	Maximum	Variance
0.107	6.186	7.560	7.359	8.756	13.35	4.035

Comparing the average per-field crop yield reported by the farmer with the yield estimated

Table 2.1: List of spectral bands of the S2-satellites. Each band has its center at the wavelength  $\lambda$  in nm with the spectral width  $\Delta\lambda$  in nm with a spatial resolution  $SR$  in m (Jaramaz et al., 2013).

Band	$\lambda$	$\Delta\lambda$	$SR$	Purpose
1	443	20	60	Atmospheric correction (aerosol scattering)
2	490	65	10	Sensitive to vegetation senescing, carotenoid, browning, and soil background; atmospheric correction (aerosol scattering)
3	560	35	10	Green peak, sensitive to total chlorophyll in vegetation
4	665	30	10	Maximum chlorophyll absorption
5	705	15	20	Position of red edge; consolidation of atmospheric corrections / fluorescence baseline.
6	740	15	20	Position of red edge, atmospheric correction, retrieval of aerosol load.
7	783	20	20	Leaf Area Index (LAI), edge of the Near-Infrared (NIR) plateau.
8	842	115	10	LAI
8a	865	20	20	NIR plateau, sensitive to total chlorophyll, biomass, LAI and protein; water vapor absorption reference; retrieval of aerosol load and type.
9	945	20	60	Water vapor absorption, atmospheric correction.
10	1375	30	60	Detection of thin cirrus for atmospheric correction.
11	1610	90	20	Sensitive to lignin, starch and forest above ground biomass. Snow/ice/-cloud separation.
12	2190	180	20	Assessment of Mediterranean vegetation conditions. Distinction of clay soils for the monitoring of soil erosion. Distinction between live biomass, dead biomass and soil, e.g., for burn scars mapping.

Table 2.2: Overview: Scene Classification Layers (SCL)

Color	No.	Class	Color	No.	Class
[Black]	0:	Missing Data	[Blue]	6:	Water
[Red]	1:	Saturated or defective pixel	[Dark Gray]	7:	Cloud low probability
[Dark Gray]	2:	Dark features / Shadows	[Light Gray]	8:	Cloud medium probability
[Brown]	3:	Cloud shadows	[Light Blue]	9:	Cloud high probability
[Green]	4:	Vegetation	[Cyan]	10:	Thin cirrus cloud
[Yellow]	5:	Bare soils	[Pink]	11:	Snow or ice

by the combine harvester shows that the latter overestimates crop yield by ca. 10% (Perich et al., 2022). Since the relative estimation error is approximately constant and we do not aim for an absolute yield prediction, we will not consider this deviation.

### 2.3 Normalized Difference Vegetation Index

The well-known NDVI introduced by Rouse (1974) is used to detect vegetation and to estimate photosynthetic activity in remote sensing (Gamon et al., 1995). It utilizes the fact that healthy, photosynthesizing vegetation exhibits a large increase in reflectance between the red and infrared region of the light spectrum (cf. appendix figure B.1). It is calculated using the S2 bands ‘red’ and ‘infrared’ (i.e., bands  $B4$  and  $B8$ —cf. table 2.1B4) by:

$$NDVI = \frac{B8 - B4}{B8 + B4}$$

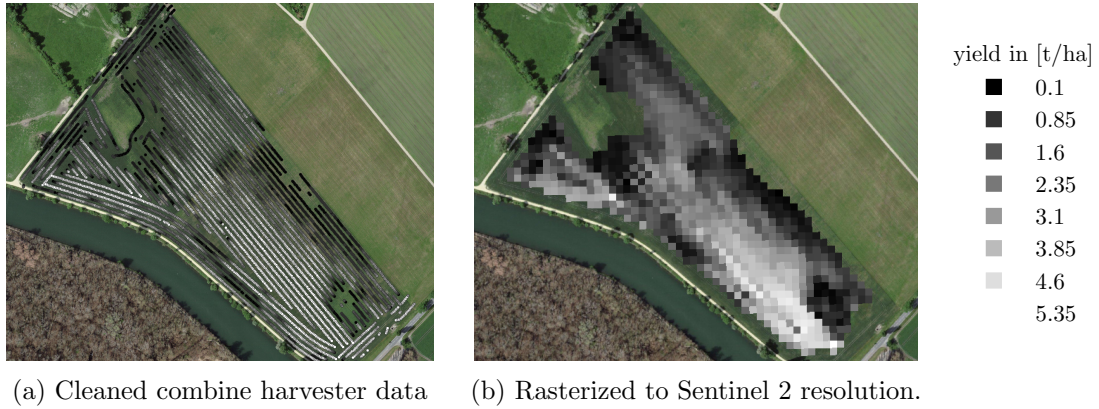


Figure 2.1: Crop yield density map of a field.

Since we measure the NDVI via the S2 satellites from space, we cannot expect to obtain the same NDVI as measured with a ground-based spectroradiometer. This is especially true if the ground signal is contaminated by either the clouds directly or by cloud shadows. Even if we only use SCL45 observations flagged as cloud-free, we still encounter measurement errors, as illustrated in section 2.6. Therefore, we call the calculated values merely the observed NDVI. In the following chapters, we will study the resulting NDVI TS extensively. Such a TS is shown in figure 2.2.

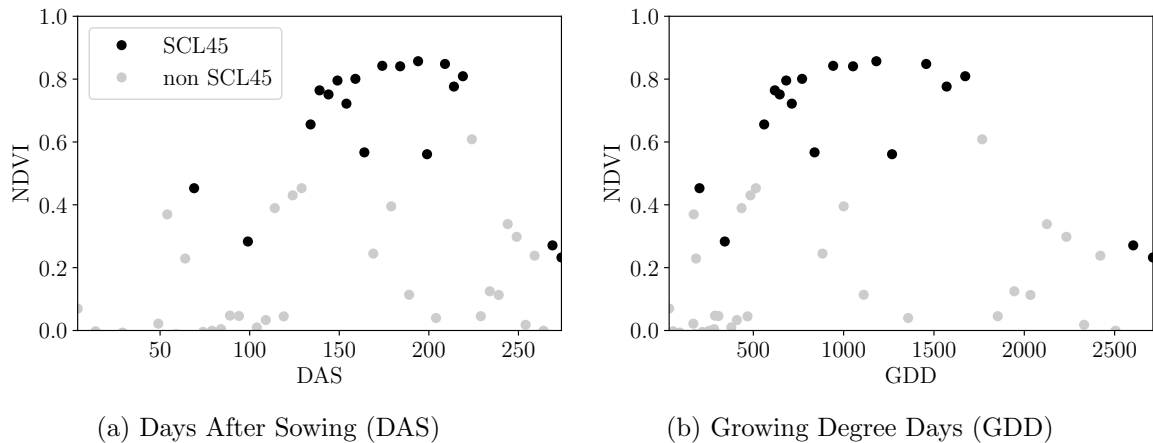


Figure 2.2: NDVI TS plotted against DAS and GDD. GDD are introduced in section 2.4.

## 2.4 Transformation of Timescale

Two drawbacks become apparent when using Days After Sowing (DAS) as the timescale (see figure 2.2a): First, this scale makes it difficult to compare two NDVI TS because wheat is not always sown on the same day of the year and in some years plants begin to emerge earlier. Second, because there are only few SCL45 observations in autumn and winter, we face significant data gaps during this period. To fix both problems, [McMaster and Wilhelm \(1997\)](#) propose to transform the timescale into a meaningful temperature based one. The resulting Growing Degree Days (GDD) are defined as the cumulative sum of temperature above a given threshold  $T_{base}$  since sowing. For cereals, we use  $T_{base} = 0$

(Holzkämper et al., 2015). Thus, the GGD for  $n$  days after sowing will be equal to

$$GDD_n := \sum_{i=0}^n \max(T_i - T_{base}, 0).$$

An example for comparison of the DAS and GDD timescale is shown in figure 2.2. Here we see that the first 120 DAS are compressed to just 500 GDD, and hence the gap in observations was successfully compressed. Given the reasons mentioned above, from now on we will only consider GDD. Important plant growth stages and their corresponding GDD values are tabulated in the appendix B.1.2.

## 2.5 The Concept of a ‘Pixel’

Now we create a new data structure that we call Pixel. This originates from the pixels of the S2 satellite images (for an illustration of such pixels, see figure 2.1b). It will contain all the information needed to answer the research questions in the following chapters.

Consider a  $10m \times 10m$  square that coincides with a S2 image pixel and  $T$  the GDD values for which S2 images are available in a given season. For  $t \in T$  let  $P_t$  be a tuple of all the spectral bands, the observed NDVI and the SCL class at the considered location at time  $t$ . Then, define the pixel  $P$  as the collection of all the  $P_t$  and the estimated dry yield for this square.

## 2.6 Illustration of S2 Images

Using an example pixel, we illustrate the challenges in working with S2 image data. Figure 2.3 shows a selection of 6 satellite images of a field, and the NDVI TS for the highlighted pixel. In February (image a), we see no vegetation but bare soil and thus also a low NDVI. At the beginning of May (b), we observe a cloudless dark green field with a high NDVI. In (c) heavy cloud cover (SCL class 9) leads to a complete loss of plant information in this S2 observation. Figure (d) shows that the SCL classification is not reliable, since we evidently observe clouds, which is also reflected in a sudden NDVI drop. Even though SCL indicates that (e) are thin cirrus clouds, a pale green shimmers through, and we also note a reasonably high NDVI. Therefore, we remark that some SCL45 observations are not accurate and even though a few non-SCL45 observations contain useful information, most of them are too unreliable (e.g., all SCL 9 observations). Thus, we aim to substitute the unreliable ones with interpolated versions and correct contaminated ones.

## 2.7 Estimation Evaluation Criteria

In this section, we define score functions to measure estimation accuracy and techniques to adequately apply them.

### 2.7.1 Score Functions

Now, we define the Root Mean Square Error (RMSE), a prominent and outlier-sensitive score function.

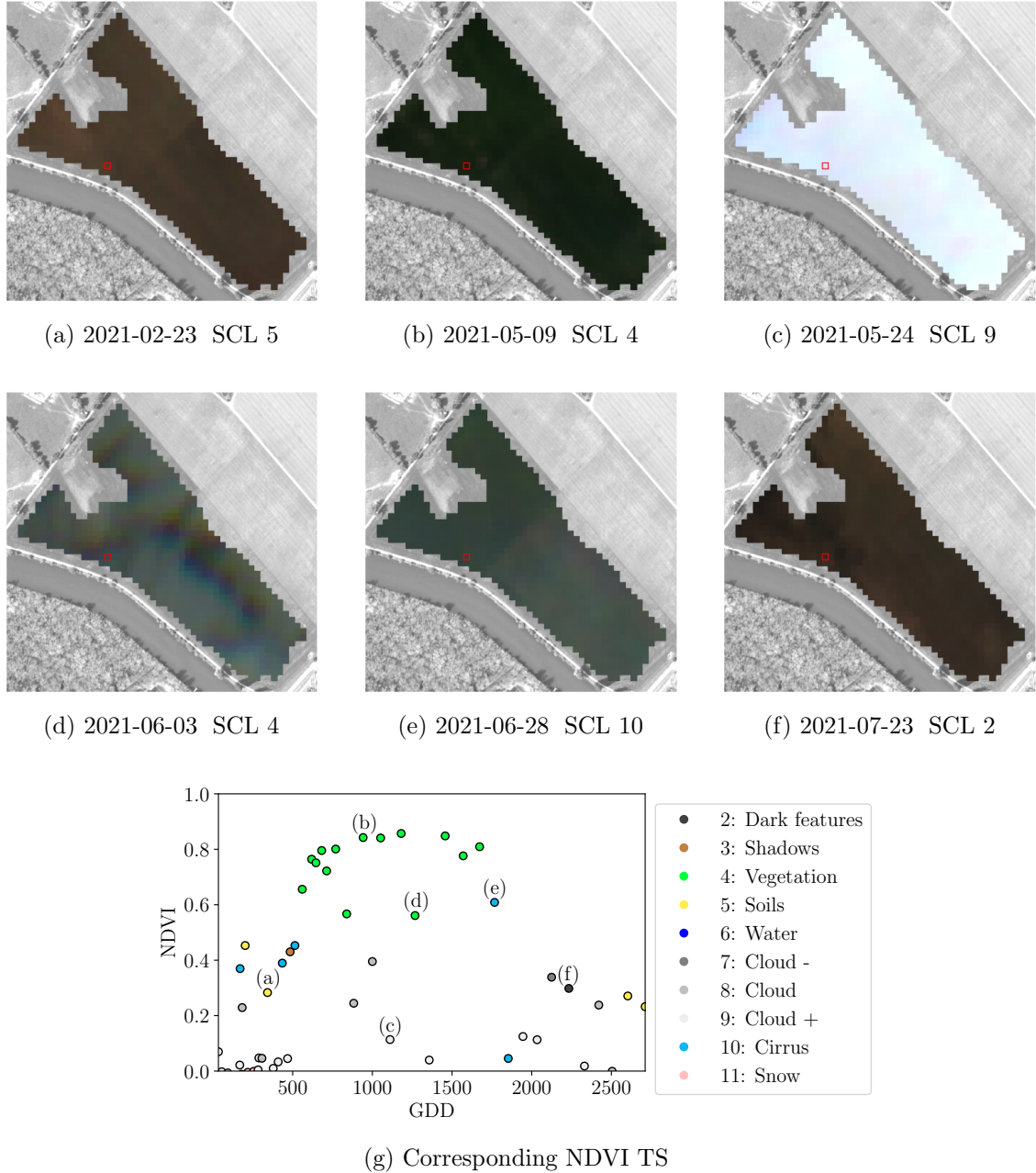


Figure 2.3: Satellite images of a field at selected times with a static grayscale background for orientation. Moreover, the NDVI TS of the red-highlighted pixel is shown in (g) colored by the SCL labels.

**Definition 2.7.1.1.** (*RMSE*) Given a vector  $y \in \mathbb{R}^n$  and its estimator  $\hat{y}$ , we define the RMSE as

$$\text{RMSE} := \sqrt{\frac{1}{n} \sum_{i=1}^n (y_i - \hat{y}_i)^2}$$

Thus, the RMSE measures how close the estimated  $\hat{y}$  are to the original  $y$  by considering the squares of errors. The lower the RMSE, the closer are the fitted values to the original values. Note that one strong outlier may corrupt this score function. Therefore, we will also define the  $x^{\text{th}}\%$  Quantile of Absolute Residuals (QAR $^x$ ) that can handle some fraction of outliers:

**Definition 2.7.1.2.** (*QAR $^x$* ) Given a percentage  $x \in \{1, 2, \dots, 100\}$ , a vector  $y \in \mathbb{R}^n$  and its estimator  $\hat{y}$ , assume without loss of generality that  $|y_1 - \hat{y}_1| \leq |y_2 - \hat{y}_2| \leq \dots \leq |y_n - \hat{y}_n|$ . Then, we define the QAR $^x$  as the biggest residual under the  $x\%$  smallest ones. Formally:

$$\text{QAR}^x := \max \left\{ |y_i - \hat{y}_i| : i \leq \frac{x}{100} n \right\}$$

Note that QAR $^{50}$  coincides with the median of absolute residuals and QAR $^{100}$  with the maximum of absolute residuals. Hence, the higher  $x$ , the fewer outliers QAR $^x$  can handle. Consequently, if we expect the data to have 5% outliers, we should choose  $x$  smaller than 95. Furthermore, if an estimator attains lower QAR $^x$  values than a competing estimator for  $x = 50, 75, 85$ , we conclude<sup>1</sup> that it also produces smaller residuals in most cases.

### 2.7.2 Out-Of-Bag and Leave-One-Out-Cross-Validation

The rationale for Out-Of-Bag (OOB) and Leave-One-Out-Cross-Validation (LOOCV) is that we intend to evaluate a model  $M$  with unseen data. That is, if  $D$  describes the entire dataset, and we train a model on a subset of  $D$ , we can use the remaining data to evaluate the model. To formally introduce this, let

$$D := \{(X_{[j,:]}, y_j) \mid X \in \mathbb{R}^{n \times p}, y \in \mathbb{R}^n, j = 1, \dots, n\}$$

be a dataset,  $i \in \{1, \dots, n\}$  and  $M^{(-i)}$  a model fitted on a subset of  $D \setminus \{(X_{[i,:]}, y_i)\}$ . Then we call  $\hat{y}_i := M^{(-i)}(X_{[i,:]})$  an OOB estimator of  $y_i$ . If we do this for all  $i \in \{1, \dots, n\}$ , we obtain  $\hat{y} := (\hat{y}_1, \dots, \hat{y}_n)$  the OOB estimator for  $y \in \mathbb{R}^n$ .

In the case that  $M^{(-i)}$  was fitted on the set  $D \setminus \{(X_i, y_i)\}$  (i.e., not a true subset), we call the corresponding  $\hat{y}_i$  also the LOOCV estimator. If we optimize some parameter via OOB (or LOOCV) this means that we search for the parameter that minimizes some loss function which takes the OOB (or LOOCV) residuals. In the bootstrap (e.g., random forest) framework, we define  $\hat{y}_i$  to be the average of all computed and feasible  $M^{(-i)}$ .

---

<sup>1</sup>Strictly speaking, this conclusion assumes that the distribution of the residuals have a similar shape and that they are unimodal (i.e., has only one ‘peak’).

# Chapter 3

## Interpolation

The need for interpolating the NDVI TS was established in the previous chapter. In this chapter, we first specify a setting for the interpolation and categorize the IMs into those that make fundamental shape assumptions (parametric) and those that are more flexible (non-parametric). We give an introduction for each method with a compact definition, highlight adjustments or give remarks where appropriate, and point out strengths and weaknesses of each method. A brief overview of the considered IMs is provided in table 3.1. Afterwards, we extract a robustification strategy from one IM and generalize it, so we can use it for all methods that allow for a priori weighted observations. Finally, using LOOCV, we tune the parameters (where necessary) and get a first idea of the performance of each method.

### 3.1 Interpolation Setup

Data is given in the form of  $(t_i, y_i)$  for  $i = 1, \dots, n$  where  $t_i$  is the time in GDD and  $y_i$  denotes the NDVI at  $t_i$ . We assume that it can be represented by

$$y_i = m(t_i) + \varepsilon_i,$$

where  $\varepsilon_i$  is some random noise and  $m : \mathbb{R} \rightarrow \mathbb{R}$  is some (parametric or non-parametric) function. If we assume that  $\varepsilon_1, \dots, \varepsilon_n$  i.i.d. with  $\mathbb{E}[\varepsilon_i] = 0$  then

$$m(t) = \mathbb{E}[y | t]$$

We will introduce parametric and non-parametric approaches to estimate  $m$  in section 3.2 and 3.3. Furthermore, we denote  $w \in \mathbb{R}^n$  as the vector of weights such that  $w_i$  corresponds to the weight that  $(t_i, y_i)$  should have in the interpolation. Since not all the following IMs support extrapolation outside the data range, we will always extrapolate with the closest value within the data range. To increase data quality, we will only consider SCL45 observations for now.

### 3.2 Parametric Regression

Parametric Curve estimation tries to fit a parametric function to a dataset, such as, a Gaussian function with parameters  $\mu$  and  $\sigma$ . In the following, we introduce two parametric approaches.

### 3.2.1 Double Logistic

The Double Logistic (DL) smoothing as described in Beck et al. (2006) heavily relies on shape assumptions of the fitted curve (i.e., the NDVI TS). First, we assume that there is a minimum NDVI level  $y_{\min}$  in the winter (e.g., due to evergreen plants), which might be masked by snow. This can be estimated beforehand, taking several years into account. Second, we assume that the growth cycle can be divided into an increase and a decrease period, where both follow a logistic function. The fastest increase (or decrease) is observed at  $t_0$  (or  $t_1$ ) with a slope of  $d_0$  (or  $d_1$ ). The equation of the double-logistic fit is given by:

$$y(t) = y_{\min} + (y_{\max} - y_{\min}) \left( \frac{1}{1 + e^{-d_0(t-t_0)}} + \frac{1}{1 + e^{-d_1(t-t_1)}} - 1 \right)$$

Where the five free parameters:  $y_{\max}$ ,  $d_0$ ,  $d_1$ ,  $t_0$ ,  $t_1$  are estimated by least squares. Such fit can be seen in figure 3.1.

#### Robustification

Similar as for the SG (introduced in section 3.3.3), one can reestimate the parameters by giving less weight to the overestimated observations and more weight to the underestimated observations. For the details on the choice of the weights, we refer to Beck et al. (2006). We will not apply this reestimation, but rather the robustification introduced later in section 3.5.

Strengths	Weaknesses
<ul style="list-style-type: none"> <li>— Incorporates subject specific knowledge in the case of evergreen plants covered in snow.</li> <li>— Optimized parameters have an intuitive meaning.</li> <li>— Robust due to shape assumptions.</li> <li>— Meaningful parameters.</li> </ul>	<ul style="list-style-type: none"> <li>— Strong shape assumptions limit flexibility.</li> <li>— Parameter estimation can go wrong. Introducing bounds can help.</li> </ul>

### 3.2.2 Fourier Series

Stöckli and Vidale (2004) approximates the NDVI curve using a second order Fourier Series (FS):

$$\text{NDVI}(t) = \sum_{j=0}^2 \left( a_j \cos(j\Phi_t) + b_j \sin(j\Phi_t) \right)$$

where  $\Phi_t = T(t-1)/(2\pi n)$ . If we set the period  $T$  to match one year, this would coincide with the notion that plants grow every year. Analogous to section 3.2.1 we fit the function above to the data via least squares. Example fits can be seen in figure 3.1.

Strengths	Weaknesses
<ul style="list-style-type: none"> <li>— Assumption of periodicity can be helpful if we are modelling multiyear growth cycles.</li> <li>— Fourier Series are popular.</li> </ul>	<ul style="list-style-type: none"> <li>— Bad behavior in regions with little data (cf. figure 3.1).</li> <li>— Hard to interpret estimated parameters.</li> <li>— Parameter estimation can go wrong. Introducing bounds can help.</li> </ul>

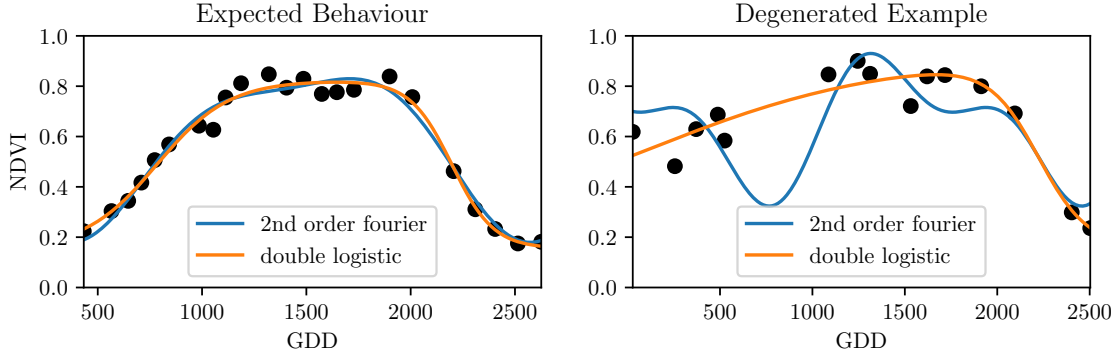


Figure 3.1: Here we observe the possibilities of a precise fit for the two parametric methods, but notice also some misbehavior.

### 3.2.3 Optimization Issues

We shall mention some optimization issues we countered during implementation. Since we aim to minimize the residual sum of squares over 5 (or 6) parameters, we try to solve a non-convex optimization problem. Thus, the algorithm<sup>1</sup> either struggles to find the global minimum or fails to converge. This was fixed by providing for each parameter reasonable initial values and generous bounds that match our experience (cf. appendix section B.2.1 for the bounds).

## 3.3 Non-Parametric Regression

In non-parametric curve estimation, the curve does no longer have to be fully determined by parameters, but we allow it to flexibly approximate the data. Note that this does not exclude tuning-parameters.

### 3.3.1 Kernel Regression: Nadaraya-Watson

As described in section 3.1, we aim to estimate

$$\mathbb{E}[Y \mid T = t] = \int_{\mathbb{R}} y f_{Y|T}(y \mid t) dy = \frac{\int_{\mathbb{R}} y f_{T,Y}(t, y) dy}{f_T(t)}, \quad (3.3.1.1)$$

where  $f_{Y|T}$ ,  $f_{T,Y}$ ,  $f_T$  denote the conditional, joint and marginal densities. This can be done with a kernel  $K$

$$\hat{f}_T(t) = \frac{\sum_{i=1}^n K\left(\frac{t-t_i}{h}\right)}{nh}, \quad \hat{f}_{T,Y}(t, y) = \frac{\sum_{i=1}^n K\left(\frac{t-t_i}{h}\right) K\left(\frac{y-Y_i}{h}\right)}{nh^2}, \quad (3.3.1.2)$$

where  $h$ , the bandwidth, symbolizes the window size of observations to consider. By using the above function in equation (3.3.1.1), we arrive at the Nadaraya-Watson kernel estimator (NW):

$$\hat{m}(t) = \frac{\sum_{i=1}^n K((t - t_i)/h) Y_i}{\sum_{i=1}^n K((t - t_i)/h)}$$

Common choices for the kernel are the normal function or a uniform function (also called ‘box’ function).

<sup>1</sup>We used the python function `scipy.optimize.curve_fit`.

### Choose Bandwidth

Note, that we still need to choose the bandwidth of the function. This can be done with the help of LOOCV while optimizing the RMSE. For non-equidistant data we refer to [Brockmann et al. \(1993\)](#) where a local adaptive bandwidth selection is presented.

Strengths	Weaknesses
— Flexible due to different possible kernels.	— $\hat{m}$ is only continuous if $t \mapsto K(t)$ is continuous.
— Can be assigned degrees of freedom.	— Choice of bandwidth, especially if $t_i$ are not equidistant.
— Estimation of the noise variance $\hat{\sigma}_\varepsilon^2$ . <sup>2</sup>	— Biased estimator. Underestimation (overestimation) for peaks (valleys).

### 3.3.2 Universal Kriging

Universal Kriging (UK) as described in [Diggle and Ribeiro \(2007\)](#) was developed in geostatistics to deal with autocorrelation of the response variable at locations that are spatially close. By applying the notion that two spectral indices that are timewise close should also take similar values, we justify the application of UK. In the end, we would like to fit a smooth Gaussian process to the data.

A Gaussian Process  $\{S(t) : t \in \mathbb{R}\}$  is a stochastic process if  $(S(t_1), \dots, S(t_k))$  has a multivariate Gaussian distribution for every collection of times  $t_1, \dots, t_k$ .  $S$  can be fully characterized by the mean  $\mu(t) := E[S(t)]$  and its covariance function  $\gamma(t, t') := \text{Cov}(S(t), S(t'))$ . Furthermore, we will assume the Gaussian process to be stationary. That is for  $\mu(t)$  to be constant in  $t$  and  $\gamma(t, t')$  to depend only on  $h = t - t'$ . Thus, we will write in the following only  $\gamma(h)$ .<sup>3</sup> Now, we need to make some assumptions on the covariance function. For this we introduce the Variogram of a Gaussian process as

$$V(h) := V(t, t + h) := \frac{1}{2} \text{Var}(S(t) - S(t + h)) = \gamma(0) + \gamma(t)$$

and define  $\gamma$  via the above equation by choosing the Gaussian Variogram defined by

$$V(h) = p \cdot \left( 1 - e^{-\frac{h^2}{(\frac{4}{7}r)^2}} \right) + n.$$

Here  $h$  denotes the distance,  $n$  is the nugget,  $r$  is the range and  $p$  is the partial sill. The influence of the parameters is visualized in figure 3.2.<sup>4</sup> Finally, we consider a one-dimensional Gaussian process  $G_\gamma$  with Variogram  $\gamma$  and tune the Variogram parameters using maximum likelihood. As illustrated in figure 3.3 maximum likelihood estimation can lead to overfitting. Thus, we will in practice sample several such optimized parameters and use their median in the end. Let  $z$  be a vector with the new values to extrapolate, then we can determine the values  $m(z) = \mathbb{E}[G_\gamma(z)|(t, y)]$  using Bayes rule<sup>5</sup>. For an example fit, we refer to figure 3.3.

<sup>2</sup>Cf. lecture notes of [Bühlman and Maechler \(2020\)](#) section 3.2.2.

<sup>3</sup>Note that the process is also isotropic (i.e.,  $\gamma(h) = \gamma(\|h\|)$ ) since we are in a one-dimensional setting and the covariance is symmetric.

<sup>4</sup>Strictly speaking, we use a scaled version of the Variogram. Thus, only the ratio of  $p/n$  matters.

<sup>5</sup>Bayes rule claims that for two random variables  $A$ , and  $B$  we have that  $P(A|B) = P(B|A)/P(B)$ .

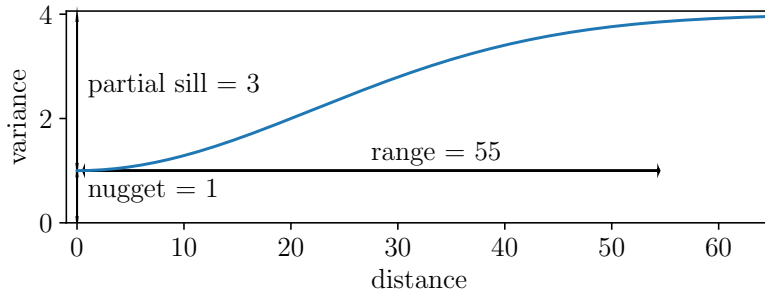


Figure 3.2: Gaussian Variogram with nugget=1, partial sill=3, range=55

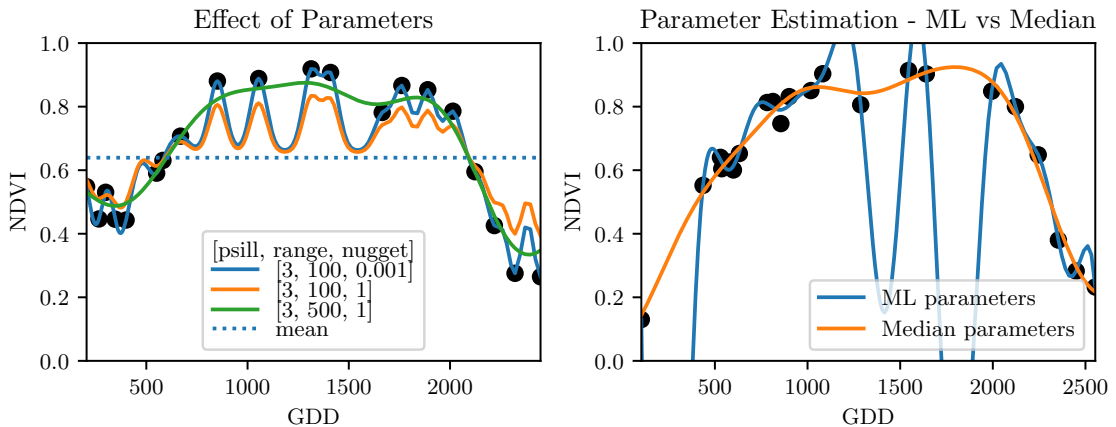


Figure 3.3: On the left, we see how the interpolation changes if we increase the nugget and the range parameter. On the right, we compare two UK interpolations, where one takes parameters by numerically maximizing the (which results in a very small nugget) and the other takes the median of many such numerical optimizations.

### Violated Assumption

Since we observe a clear pattern of a growth period in spring and harvest in the end of summer, we conclude that our stationarity assumption with the constant mean is structurally violated. This is also why we observe a tendency to the mean, as indicated in figure 3.3, regardless of range parameter.

Strengths	Weaknesses
<ul style="list-style-type: none"> <li>— It is a well-studied method.</li> <li>— Informative variogram parameters.</li> <li>— Flexible covariance structure.</li> </ul>	<ul style="list-style-type: none"> <li>— Violated stationarity assumption (constant mean and constant variance).</li> <li>— Tendency to the mean (especially within data gaps).</li> <li>— Pure maximum likelihood can result in overfitting.</li> </ul>

### 3.3.3 Savitzky-Golay Filter

The Savitzky-Golay Filter (SG), introduced in [Savitzky and Golay \(1964\)](#) is a technique in signal processing and can be used as a low-pass filter ([Schafer, 2011](#)). Hence, it can also

be used for smoothing by filtering high frequency noise while keeping the low frequency signal.

First, we choose a window size  $m$ . Then, for each point,  $j \in \{m, m+1, \dots, n-m\}$  we fit a polynomial of degree  $k$  by:

$$\hat{y}_j = \min_{p \in P_k} \sum_{i=-m}^m (p(t_{j+i}) - y_{j+i})^2,$$

where  $P_k$  denotes the Polynomials of degree  $k$  over  $\mathbb{R}$ . For equidistant points this can efficiently be calculated by

$$\hat{y}_j = \sum_{i=-m}^m c_i y_{j+i},$$

where the  $c_i$  are only dependent on the  $m$  and  $k$  and are tabulated in the original paper.

[Chen et al. \(2004\)](#) developed a ‘robust’ IM variant of the SG. The method is based on the assumption that due to atmospheric effects the observed NDVI tends to be underestimated and that it cannot increase too quickly. The latter is argued by the biological impossibility of such fast vegetation changes. Their proposed algorithm is:

- i.) Remove non-SCL45 points.
- ii.) Remove points that would indicate an increase greater than 0.4 within 20 days.
- iii.) Linearly interpolate to obtain an equidistant TS  $X^0$ .
- iv.) Apply the SG to obtain a new TS  $X^1$ .
- v.) Set  $X^0 \leftarrow X^1$  and update  $X^1$  by applying again the SG. Repeat this until  $w^T |X^1 - X^0|$  stops decreasing, where  $w$  is a weight vector that is only used for evaluation and not for fitting and is calcualted by  $w_i = \min \left( 1, 1 - \frac{X_i^1 - X_i^0}{\max_i \|X_i^1 - X_i^0\|} \right)$ . This reduces the penalty introduced by outliers<sup>6</sup> and by repeating this step we approach the ‘upper NDVI envelope’.

### Extension: Spatial-Temporal SG

One notable adaptation of the SG is the presented by [Cao et al. \(2018\)](#). The key difference is the additional assumption of the cloud cover being discontinuous and that we can improve by looking at adjacent<sup>7</sup> pixels. Because we are working with rather high-resolution satellite data, and we need the variance in the predictors, we will waive this extension.

<sup>6</sup>Here we call a point  $i$  an outlier if  $X_i^0 < X_i^1$ .

<sup>7</sup>Here, we say that a pixel is adjacent if it is the same pixel but from a different year (keeping the same day of the year) or (if not enough of such temporal-adjacent pixel are found) it is spatially adjacent.

Strengths	Weaknesses
<ul style="list-style-type: none"> <li>— Popular technique in signal processing.</li> <li>— Efficient calculation for equidistant points.</li> <li>— The upper envelope matches intuition for the NDVI. Therefore, it is robust against outliers with small values.</li> </ul>	<ul style="list-style-type: none"> <li>— No natural way of how to estimate points that are not in the data.</li> <li>— Not generalizable to other spectral indices.</li> <li>— Linear interpolation to account for missing data might not be appropriate.</li> <li>— No continuous interpolation between two measurements.</li> </ul>

### 3.3.4 Locally Weighted Regression

The Locally Weighted Regression (LOESS) introduced by [Cleveland \(1979\)](#) can be understood as a generalization of the SG (cf. section 3.3.3).

Given a proportion  $\alpha \in (0, 1]$ , we estimate each  $y_i$  separately by fitting a polynomial of order  $d$  by weighted least squares. The weights are usually<sup>8</sup> defined by

$$w_i(t_j) = \begin{cases} \left(1 - \left(\frac{|t_j - t_i|}{h_i}\right)^3\right)^3, & \text{for } |t_j - t_i| < h_i, \\ 0, & \text{for } |t_j - t_i| \geq h_i \end{cases}$$

where  $h_i$  is the minimal distance such that  $\lceil \alpha n \rceil$  observations are in the ball  $B_{h_i}(t_i)$ .<sup>9</sup> So for each  $y_i$ , we only consider a proportion  $\alpha$  of the observations.

#### Differences between the Robust LOESS and the SG

The LOESS smoother takes a fraction of points instead of a fixed number, and therefore automatically adapts to the size of the data we wish to interpolate. However, we run into the danger of considering too little observations, since the estimation breaks down if  $\lceil \alpha n \rceil < d + 1$ .<sup>9</sup> Furthermore, LOESS gives less weight to points further away. This yields a ‘smoother’ estimate, since when we slide the window (e.g., for estimating the next value) an influential point at the border does not suddenly get zero weight from being weighted equally before. Finally, the LOESS can also be used for non-equidistant data and allows for arbitrary interpolation.

Strengths	Weaknesses
<ul style="list-style-type: none"> <li>— Flexible generalization of SG.</li> <li>— Arbitrary interpolation possible.</li> <li>— Intuitive parameters.</li> </ul>	<ul style="list-style-type: none"> <li>— The nature of local regression might lead to surprising estimates (no smoothness guarantees for the second derivative).</li> </ul>

<sup>8</sup>Other functions are also possible choices as long as they satisfy the conditions stated in [Cleveland \(1979\)](#).

<sup>9</sup>If too many weights are set to zero, we might end up considering not enough observations and thus get a singular design-matrix (for the least squares estimation). To extend good behavior, we substitute  $h_i$  with  $1.01h_i$ , so that the observations on the boundary of  $B_{h_i}(t_i)$  do not get completely ignored. But we also have to assure that  $\alpha$  is big enough.

### 3.3.5 B-Splines

B-Splines (BS) as discussed in [Lyche and Mørken \(2005\)](#) are piecewise cubic polynomials defined by

$$S(t) = \sum_{j=0}^{n-1} c_j B_{j,k;t}(t),$$

where  $B$  are basis functions and recursively defined by

$$B_{i,0}(z) = 1, \text{ if } t_i \leq z < t_{i+1}, \text{ otherwise } 0$$

$$B_{i,k}(z) = \frac{z - t_i}{t_{i+k} - t_i} B_{i,k-1}(z) + \frac{t_{i+k+1} - z}{t_{i+k+1} - t_{i+1}} B_{i+1,k-1}(z).$$

Assuming that all  $t_i$  are distinct, this yields an interpolation that fits the data perfectly. To reduce the amount of overfitting and increase the smoothness, we relax the constraint that we must interpolate perfectly. Thus, we use the minimum number of basis functions<sup>10</sup> such that keeps the sum of squares below some threshold  $\lambda$ :

$$\sum_{i=1}^n (w_i(y_i - \hat{y}_i))^2 \leq \lambda$$

Strengths	Weaknesses
— Can be assigned degrees of freedom.	— Smoothing process does not translate well to an interpretation (unlike SS).
— Extendable to a ‘smooth’ version.	
— Also performs well if points are not equidistant.	— Choice of smoothing parameter $\lambda$ .

### 3.3.6 Smoothing Splines

To define Smoothing Splines (SS) as in [Craven and Wahba \(1978\)](#), let  $\mathcal{F}$  be the Sobolev space (i.e., the space of functions for which the second derivative is integrable). Then SS are the unique minimizer of

$$\arg \min_{f \in \mathcal{F}} \sum_{i=1}^n w_i (y_i - f(t_i))^2 + \lambda \int f''(t)^2 dt, \quad \text{for } \lambda > 0. \quad (3.3.6.1)$$

The objective function ensures that we decrease the curvature while keeping the RMSE low. SS can be represented as cubic splines i.e., piecewise cubic polynomial functions.

#### Whittaker — Discrete Version with Higher Order Derivatives

The Whittaker smoother introduced in [Eilers \(2003\)](#) is closely reminiscent of the SS and is also used for the NDVI TS ([Atzberger and Eilers, 2011](#)). Similar to SS, we minimize the following expression:

$$\arg \min_{z \in \mathbb{R}^n} (y - z)^T W (y - z) + \lambda z^T D^T D z,$$

<sup>10</sup>So we do not require one basis function for each neighboring pair of knots. SciPy uses FITPACK and DFITPACK, the documentation suggests that smoothness is achieved by reducing the number of knots used.

where  $W$  is a diagonal weight-matrix,  $\lambda$  our smoothing parameter and  $D$  a matrix that serves the purpose of approximating a differentiation of  $k^{\text{th}}$  order. In essence, this minimization function is the same as equation 3.3.6.1. The only differences are, that we substitute the integral by a sum and that we are more flexible with the order of the derivatives we are using. The main drawback is that we do not get a smooth function that interpolates, and that the sum behaves worse than the integral for non-equidistant data points. Thus, we will not consider the Whittaker further in favor of the more general SS.

Strengths	Weaknesses
<ul style="list-style-type: none"> <li>— Can be assigned degrees of freedom.</li> <li>— Efficient estimation (closed form solution).</li> <li>— Intuitive penalty reduces curvature.</li> <li>— Performs well if points are not equidistant.</li> <li>— Fixes the Runge's phenomenon.<sup>11</sup></li> <li>— Bounded within the data range if <math>\lambda</math> is chosen a priori.</li> </ul>	<ul style="list-style-type: none"> <li>— The tuning parameter <math>\lambda</math> must be chosen. This can be done via cross validation and optimizing a score function (e.g., the RMSE).</li> </ul>

## 3.4 Tuning Parameter Estimation

Many of the IMs introduced in section 3.2 and 3.3 include a free parameter. To determine this parameter for a specific IM, we will estimate the absolute residuals using OOB estimation and then optimize the parameter using a score function. We clarify the procedure step by step:

- i.) Construct a set  $\Lambda$  of candidate parameters that generously covers the parameter space.
- ii.) Consider the vector  $z := (y_1^{(1)}, \dots, y_{n_1}^{(1)}, y_1^{(2)}, \dots, y_{n_2}^{(2)}, \dots, y_1^{(m)}, \dots, y_{n_m}^{(m)})$  of all NDVI TS for all  $m$  pixels.
- iii.) Consider its LOOCV estimator  $\hat{z}_\lambda$  using the specific IM and the parameter  $\lambda$  for each pixel individually.
- iv.) Determine  $\lambda_{optimal} = \arg \min_{\lambda \in \Lambda} \text{QAR}^{90}(\hat{z}_\lambda)$

We choose  $\text{QAR}^{90}$  as our optimization function because we want to allow 10% of outliers (contaminated points) but also aim for an accurate fit in 90% of the cases. Figure 3.4 exemplifies the effect of the chosen quantile in the optimization function ( $\text{QAR}^x$ ). To summarize, we may say that the higher the quantile, the stronger the smoothing.

## 3.5 Robustification

Now we discuss a general approach of how to make an interpolation more robust against outliers. The main idea is to give less weight to observations that have high residuals after the initial (or when reiterating, the previous) fit. Even though the procedure is taken from the robust version of the LOESS smoother (cf. section 3.3.4 and Cleveland (1979)), we

<sup>11</sup>I.e., fluctuation of high degree polynomial interpolation.

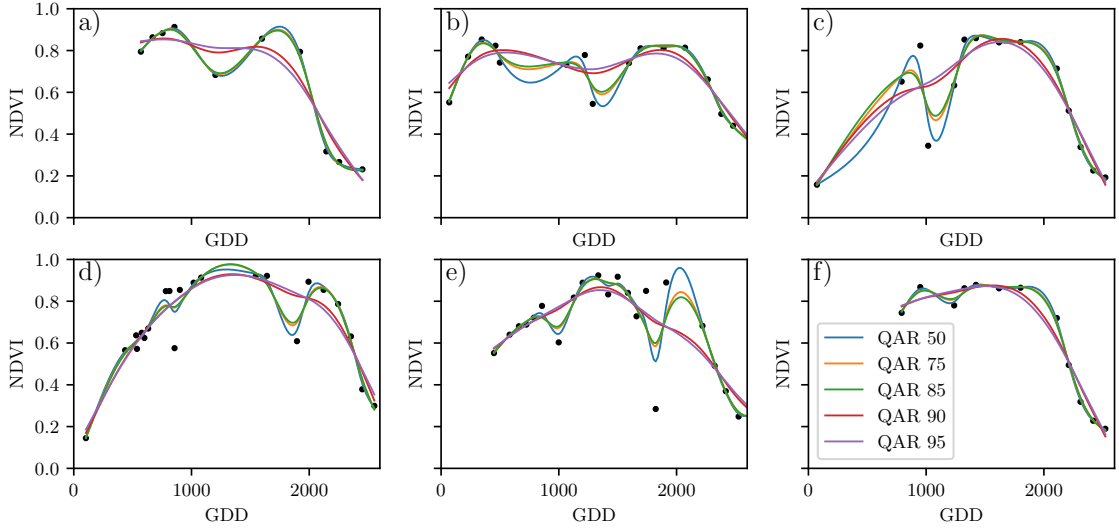


Figure 3.4: Smoothing splines fit with smoothing parameter optimized by minimizing the LOOCV QAR. Note that the larger the considered quantile is, the more the curvature of the resulting curve decreases.

can apply it to every IM that allows for prior weighting of observations. After an initial fit, we calculate the residuals  $r_i := y_i - \hat{y}_i$  and obtain  $\tilde{r}_i$  by scaling with the median of the absolute residuals

$$\tilde{r}_i := \frac{r_i}{6 \text{ med}(|r_1|, \dots, |r_n|)}$$

Next, we compute new weights by

$$w_i^{\text{new}} := \begin{cases} w_i^{\text{old}} (1 - \tilde{r}_i^2)^2 & \text{if } |\tilde{r}_i| < 1 \\ 0 & \text{else} \end{cases} \quad (3.5.0.1)$$

Using the new weights, we can re-interpolate. This reweighting can be iterated for a fixed number of steps or till the change of the values is smaller than some tolerance. This procedure is indeed robust since we use the median for the normalization which has a breakdown point<sup>12</sup> of 50%.<sup>13</sup>

### 3.5.1 Our Adjustment:

During the iterations or when supplying prior weights, low-weighted observations can corrupt our estimation of scale (the median of absolute residuals). Thus, we will use the weighted median defined by

$$\text{med}_{\text{weighted}}(r, w) := \arg \min_{\lambda \in \mathbb{R}} \sum_{i=1}^n |r_i w_i - \lambda|, \quad \text{for } r, w \in \mathbb{R}^n.$$

<sup>12</sup>Intuitively, the breakdown point denotes the fraction of observations a ‘vicious’ player can replace without breaking the estimator. For example, the median has a breakdown point of 50%.

<sup>13</sup>The breakdown point relates only to outliers in the  $y$  values. Note that we do not require the IMs to be robust, since the residual for an outlier will still be larger than for non-outliers and thus will be down weighted more and more in each iteration (because for the next iteration the residual of the outlier will be even larger, since we gave less weight to it).

### 3.5.2 Examples and Conclusions

Examples of the first four iterations using SS and LOESS are shown in figure 3.5 and 3.6 for six pixels. For the analogous figures of BS and DL, we refer to the appendix B.2 and B.3. Indeed, we observe how the interpolated TS is less affected by outliers after each iteration. The most notable change happens during the first iteration. In figure 3.5 plot (d) we see how the interpolation ‘escapes’ from the right endpoint with each successive iteration, even though our intuition does not identify this point as an outlier. Therefore, we will always stop after one iteration.

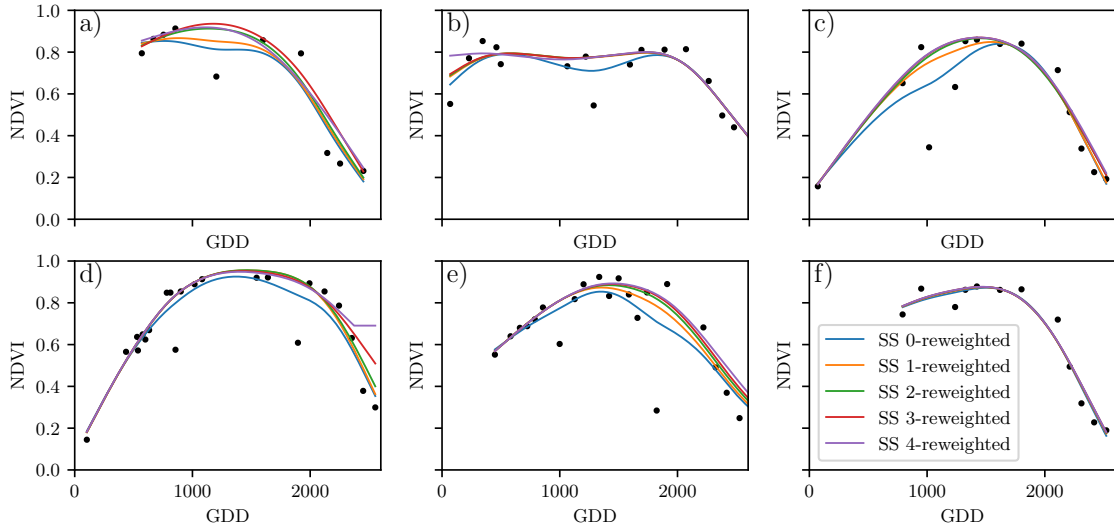


Figure 3.5: Smoothing splines fitted to different (SCL45) NDVI TS. Iterations of a robustifying refit (as indicated in section 3.5) are also displayed.

### 3.5.3 Upper Envelope Approach

If we artificially increase the negative residuals in 3.5.0.1 (e.g., by multiplying with 2), the corresponding points will get less weight in the next iteration. This allows us to create an interpolation that resembles an upper envelope. Intuitively, this upper envelope can be thought of as a sheet that is laid on top of the points. This approach is based on the premise that the observed NDVI tends to underestimate the true value (Cao et al., 2018). Since we want to develop a general method that is in principle not related to the NDVI, we will not pursue this approach further.

## 3.6 Performance Assessment

Next, we will benchmark the in section 6.1.3 preselected IMs with and without robustification. For this, we will use the same technique as we did for the parameter determination in section 3.4. We apply the score functions from section 2.7.1 on  $B_\lambda$ . The results are presented in section 5.1 and are discussed in section 6.1. The double logistic turns out to be the best convincing parametric method, and from the non-parametric methods we choose the SS.

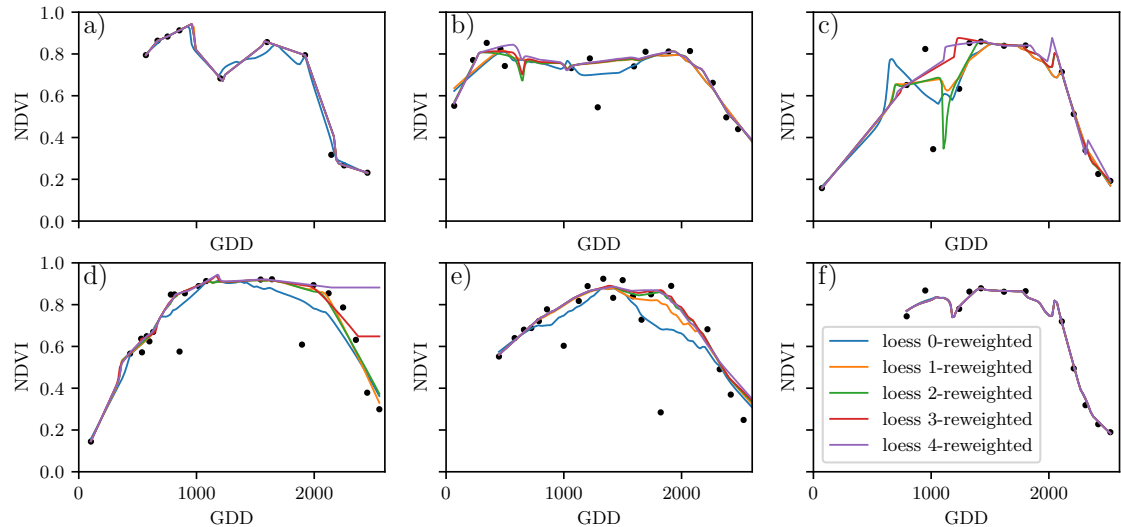


Figure 3.6: The LOESS smoother fitted to different (SCL45) NDVI TS. Iterations of a robustifying refit (as indicated in section 3.5) are also displayed.. Note the jumps in plot (c) caused by the data gap and the outlier.

Table 3.1: Overview of the studied interpolation methods containing important assumptions, strengths and weaknesses and whether the method supports weighted observations (w) and if the resulting interpolation is bounded w.r.t. a fixed interval (b).

	<b>Assumptions</b>	<b>Strengths</b>	<b>Weaknesses</b>	w	b
Double- Logistic	<ul style="list-style-type: none"> <li>- Bell shape of curve</li> <li>- NDVI has a minimal value</li> </ul>	<ul style="list-style-type: none"> <li>- Good for evergreen plants if snow masks NDVI</li> <li>- Handles data gaps well</li> </ul>	<ul style="list-style-type: none"> <li>- Parameter estimation can be challenging, to solve this the parameter space can be bounded</li> </ul>	Yes	(Yes)
Fourier Series	<ul style="list-style-type: none"> <li>- NDVI can be approximated by a 2<sup>nd</sup> order Fourier series.</li> <li>- Prominent approach</li> </ul>	<ul style="list-style-type: none"> <li>- Incorporates periodical growth-cycles</li> </ul>	<ul style="list-style-type: none"> <li>- Curve easily exceeds the bounds of the NDVI within data gaps</li> <li>- Parameter estimation can be challenging, to solve this the parameter space can be bounded</li> </ul>	Yes	No
Nadaraya- Watson	<ul style="list-style-type: none"> <li>- Close points are related to each other via a kernel function</li> </ul>	<ul style="list-style-type: none"> <li>- Simple</li> <li>- Computationally very fast</li> </ul>	<ul style="list-style-type: none"> <li>- Biased, especially at ‘peaks’ and ‘valleys’</li> <li>- Bandwidth: fails if there are big data-gaps</li> </ul>	Yes	Yes
Universal Kriging	<ul style="list-style-type: none"> <li>- Function is a realization of a stationary Gaussian process</li> </ul>	<ul style="list-style-type: none"> <li>- Informative parameters</li> <li>- Flexible</li> </ul>	<ul style="list-style-type: none"> <li>- Assumption not met for NDVI TS</li> <li>- Regression to the mean, especially within data gaps</li> </ul>	Yes	(Yes)
Savitzky- Golay	<ul style="list-style-type: none"> <li>- High frequencies are noise (Low-Pass-Filter)</li> <li>- Equidistant points</li> <li>- Local polynomials</li> </ul>	<ul style="list-style-type: none"> <li>- Computationally very fast</li> </ul>	<ul style="list-style-type: none"> <li>- Cannot deal natively with non-equidistant data</li> </ul>	No	(Yes)
Savitzky- Golay + NDVI	<ul style="list-style-type: none"> <li>- Upper envelope</li> <li>- Vegetation cannot grow faster than some slope</li> </ul>	<ul style="list-style-type: none"> <li>- Biological knowledge</li> </ul>	<ul style="list-style-type: none"> <li>- Bad ‘upper envelope’ since weights are not used for the estimation itself</li> </ul>	(No)	(Yes)
LOESS	<ul style="list-style-type: none"> <li>- Local polynomial with points closer to the estimated point are more important</li> </ul>	<ul style="list-style-type: none"> <li>- Flexible</li> <li>- Generalization of the Savitzky-Golay</li> <li>- Intuitive weighting function</li> </ul>	<ul style="list-style-type: none"> <li>- Computationally expensive</li> </ul>	Yes	(Yes)
B-Splines	<ul style="list-style-type: none"> <li>- Function can be approximated by a linear combination of B-splines basis functions</li> </ul>	<ul style="list-style-type: none"> <li>- General assumption</li> <li>- Flexible shape</li> </ul>	<ul style="list-style-type: none"> <li>- Unbounded</li> <li>- Non-intuitive smoothing process</li> </ul>	Yes	No
Smoothing Splines	<ul style="list-style-type: none"> <li>- 2<sup>nd</sup> derivative of function is integrable</li> </ul>	<ul style="list-style-type: none"> <li>- Intuitive meaning of penalty</li> <li>- General assumptions</li> <li>- Flexible shape</li> </ul>	<ul style="list-style-type: none"> <li>- Choice of smoothing parameter</li> </ul>	Yes	(Yes)



# Chapter 4

## NDVI Correction

Let's remind ourselves that the data from the S2 satellites is distributed with an SCL, and we therefore have some evidence about what is observed at each pixel for each sampled time (cf. table 2.2). So far, we have only considered points, labeled as cloud- and shadow-free (SCL45). However, we remind ourselves of the satellite images in figure 2.3d, where we had cloudy images despite the ‘vegetation’ label and see vegetation in figure 2.3e even though we are supposed to see ‘cirrus clouds’.

In this chapter, we will try to improve our NDVI interpolation by not relying only on the observed NDVI, but by training our own model to correct the NDVI using additional spectral bands. For this, we introduce several statistical modelling approaches and discuss the strengths and weaknesses for each of them. After correcting the observed NDVI, we will assess the uncertainties of our corrections and translate them into weights. These will be used for the subsequent interpolation. This step-by-step procedure is illustrated in the appendix figure B.4. Finally, we will evaluate which combinations of IMs and correction models perform the best.

### 4.1 Considering other SCL Classes

In figure 4.1 we plot the observed NDVI and notice that some blue points which correspond to the SCL-class 10 (thin cirrus clouds) follow the interpolated line closely. Hence, they might be useful in improving an interpolation fit.

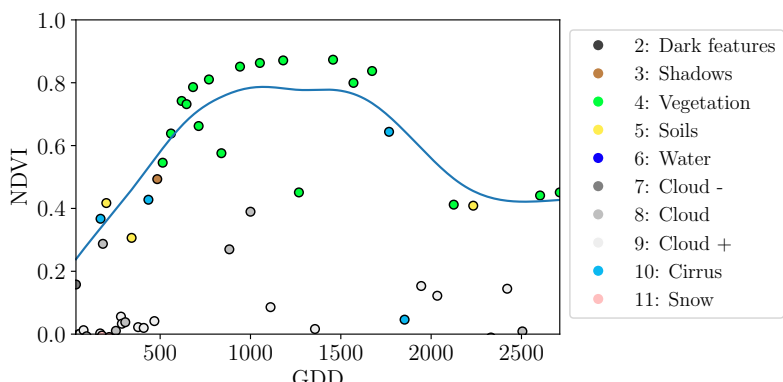


Figure 4.1: A smoothing splines fit considering green and yellow points (SCL45).

To get an impression of whether there is some useful information contained in non-SCL45 observations, we compare the observed NDVI with the true NDVI. But since we do not have any ground truth data, we will make the following assumption:

**Assumption 4.1.0.1.** The ‘true’ NDVI value at time  $t$  can be successfully estimated by a (robustified) LOOCV interpolation using high-quality observations. That is, the interpolated value using a (robustified) IM (cf. chapter 3) considering all SCL45 points except the current one. In the following, we will call this estimate the ‘true’-NDVI.

Now, we will check for the other SCL-classes if there is a relation between the ‘true’ NDVI (derived with robustified SS) and the observed NDVI. Thus, we pair each ‘true’ NDVI with its observed one, collect all pairs, and create a scatter plot for each SCL-class in fig 4.2. As expected, the ‘true’ and the observed NDVI seem to be highly correlated for SCL45. But we can also detect some patterns of correlation in the SCL-classes 2, 3, 7, 8 and 10. It might be tempting to just include some of the mentioned SCL classes for the interpolation. But on the one hand, the choice would not be objective and on the other hand, the correlation seems to be weaker than for SCL45. Therefore, in the following section, we will correct the observed NDVI and estimate the uncertainty of each correction.

## 4.2 Correction Models

For training an NDVI correction model, we require ground-truth data which we will aim to model using informative covariates. Since ground-truth NDVI data is not available, we will again use the assumption 4.1.0.1 and use the ‘true’ NDVI instead. There is no canonical answer to the question of which covariates we should use. It is a tradeoff between simplicity, generalizability, and performance (with the danger of overfitting). Our goal with the NDVI correction is to develop a product that is simple to use and to understand. Therefore, we will only utilize the spectral data of the satellite (i.e., all the bands) and the observed NDVI derived from it as covariates. We organize the chosen covariates in the design matrix  $X^1$ , where each row corresponds to a  $P_t$  (i.e., a pixel at a time  $t$ ) and each column to one covariate. In the following, we will introduce different approaches to model the relationship between the response  $y := \text{NDVI}^{\text{true}} \in \mathbb{R}^n$  and the design matrix  $X \in \mathbb{R}^{n \times p}$ . First, we will study the basic OLS. Second, we look at the LASSO, a penalized adaptation of the OLS which is known to successfully deal with highly correlated covariates. Afterwards, GAMs are introduced, which model the response similar to OLS but allow for non-linear relations. Last, we discuss RF and MARS, which are both flexible modelling approaches.

Note that in order to reduce computation time, only 10% of the data has been used to fit the subsequent models, which are still more than 120'000 observations.

### 4.2.1 Ordinary Least Squares

The Ordinary Least Squares estimator (OLS) is a linear model that aims to minimize the sum of the squared residuals. We assume a linear relationship between  $y$  and  $X$  and allow for Gaussian noise. That is:

$$y = X\beta + \epsilon \quad \text{where } \epsilon \stackrel{i.i.d.}{\sim} \mathcal{N}(0, \sigma^2)$$

---

<sup>1</sup>Strictly speaking, we include also the intercept and introduce dummy variables to encode the SCL classes.

Assuming that  $(X^T X)$  is regular, we can estimate the regression coefficients  $\beta$  by

$$\hat{\beta} = (X^T X)^{-1} X^T y = \arg \min_{\beta \in \mathbb{R}^p} \|y - X\beta\|_2.$$

We will train two models, one using all covariates discussed above ( $SCL^{all}$ ) and one using only the SCL-classes and the observed NDVI ( $SCL^{SCL}$ ).

Strengths	Weaknesses
— Simple method with good interpretability of coefficients.	— Models only linear relationships.
— Computationally cheap.	— No integrated variable selection. <sup>2</sup>

#### 4.2.2 Least Absolute Shrinkage and Selection Operator

The Least Absolute Shrinkage and Selection Operator (LASSO) can be similarly expressed than the OLS but adds a penalty to the minimization problem:

$$\hat{\beta}_\lambda = \arg \min_{\beta \in \mathbb{R}^p} \|y - X\beta\|_2^2 + \lambda \|\beta\|_1 = \arg \min_{\beta \in \mathbb{R}^p \text{ and } \|\beta\|_1 < \lambda} \|y - X\beta\|_2^2. \quad (4.2.2.1)$$

Even though we do not have a closed form solution for equation (4.2.2.1) we can solve it easily via optimization, since the function  $\beta \in \{\beta \in \mathbb{R}^p \mid \|\beta\|_1 < \lambda\} \mapsto \|y - X\beta\|_2^2$  is continuous and convex. Tibshirani (2011) shows that the LASSO solution tends to be sparse. That is  $\beta_i = 0$  for most  $i = 1, \dots, p$ . The larger  $\lambda$ , the more  $\beta_i = 0$ , and hence the simpler the resulting model. In order to know which  $\lambda$  to choose, we try a large range of possible values. For each  $\beta_\lambda$ , we calculate the cross-validated RMSE <sub>$\lambda$</sub> <sup>4</sup> (and its standard deviation  $\sigma_\lambda$  using the  $k$  folds) and define the  $\lambda$  with the smallest corresponding RMSE <sub>$\lambda$</sub>  as  $\lambda_{min}$ . From here we choose the largest  $\lambda$  for which the RMSE <sub>$\lambda$</sub>  is smaller than RMSE <sub>$\lambda_{min}$</sub>  +  $\sigma_\lambda$ . This yields a simpler model while keeping the RMSE small.

We will apply the LASSO using the selected covariates in section 4.2 and their second degree of interactions.<sup>5</sup>

Strengths	Weaknesses
— Usually yields a sparse solution. This tends to give better generalizability (prediction performance on unseen data).	— Estimate is biased.
— Successfully deals with correlation in covariates.	— Computationally expensive.
— Interpretable results.	

<sup>2</sup>There is the possibility of stepwise model selection by dropping or adding some covariates, but for higher  $p$  this gets too expensive since the time complexity grows in  $\mathcal{O}(np^4)$  (computing  $X^T X$  requires  $\mathcal{O}(np^2)$  which assuming  $n > p$  dominates  $\mathcal{O}(p^3)$  needed for the Cholesky Decomposition of  $X^T X$ ).

<sup>3</sup>The last two terms are equivalent by lagrangian optimization.

<sup>4</sup>The cross validated Root Mean Square Error is the mean of the RMSE's obtained for each fold using the model trained on the remaining folds.

<sup>5</sup>This is if our covariates are  $\{1, a, b\}$ , then we will now use  $\{1, a, b, ab, a^2, b^2\}$ .

### 4.2.3 General Additive Model

General Additive Models (GAM) as described in [Hastie and Tibshirani \(1987\)](#) are a special case of Projection Pursuit Regression, where only the  $p$  directions parallel to the coordinate axes are considered. The result is different to a linear model since the coordinate functions are not restricted to be linear but are assumed to be non-parametric functions. The model can be written as:

$$g_{add}(x) = \mu + \sum_{i=1}^p g_j(x_j).^6$$

To estimate the non-parametric functions, we can use SS (cf. section [3.3.6](#)). For this let  $\mathcal{S}_j$  be the function that takes some  $z \in \mathbb{R}^n$  and returns the SS fitted to  $(X_{:,j}, z)$  where the smoothing parameter is optimized by LOOCV<sup>7</sup>. Since we cannot fit all  $g_j$  simultaneously, we will use a strategy named Backfitting. We basically cycle through the indices  $1, \dots, p$  and refit  $\hat{g}_j$  each time. The following illustrates the procedure:

- 1)  $\hat{g}_1 = \mathcal{S}_1(y - \mu)$
  - 2)  $\hat{g}_j = \mathcal{S}_j(y - \mu - \hat{g}_1(X_{:,1}) - \dots - \hat{g}_{j-1}(X_{:,j-1})) \quad \text{for } j = 2, \dots, p$
  - 3)  $\hat{g}_1 = \mathcal{S}_1(y - \mu - \hat{g}_2(X_{:,2}) - \dots - \hat{g}_p(X_{:,p}))$
  - 4)  $\hat{g}_j = \mathcal{S}_j(y - \mu - \sum_{k \neq j} \hat{g}_k(X_{:,k})) \quad \text{for } j = 2, \dots, p$
- ⋮

We repeat step 3) and 4) until the change of the  $\hat{g}_i$ 's falls below some tolerance.

Strengths	Weaknesses
— Captures non-linearity.	— No automatic variable selection.
— Good interpretability.	— Computationally expensive.

### 4.2.4 Random Forest

To define a Random Forests (RF) introduced by [Breiman \(2001\)](#) we will first define what a Tree is. A (decision) Tree is a graph without circles, with a distinct root node, every node has at most two children and every leaf has a value assigned to it. At each non-leaf node there is a boolean condition testing if one variable is greater than some value and a pointer to one child depending on the boolean value. To evaluate a tree we start at the root node, test the boolean expression and go to the node indicated by the resulting pointer. This we repeat until we reach at a leaf, where we return the value assigned to it. To build such a Tree, we will recursively partition the covariate space using greedy splits<sup>8</sup> decreasing the RMSE<sup>9</sup> each time. If the set we want to split contains less than a certain amount of training points, we stop.

<sup>6</sup>Where  $g_j$  is a real-valued function. For identifiability we also demand  $\mathbb{E}[g_j(X_{:,j})] = 0$  for  $j = 1, \dots, p$ .

<sup>7</sup>For efficiency a proxy of the LOOCV is used called generalized cross validation.

<sup>8</sup>For computational reasons, we will only use splits along one covariate. So we ‘cut’ our covariate space into rectangles.

<sup>9</sup>To calculate the RMSE, we need a prediction. Let  $P$  be the current partition, then the predicted value for some  $x \in A \in P$  is the mean of the responses of all the points in  $A$  (included in the training data).

To build a Random Forest we will bootstrap-aggregate<sup>10</sup> many such Trees<sup>11</sup>. The prediction of the Random Forest for a new point  $x$  is then the mean of the predictions from all the Trees.

Strengths	Weaknesses
— Captures non-linear relationships.	— The resulting (prediction) function is not continuous, but locally constant.
— Captures all interactions and performs automatic variable selection.	— Computationally expensive.
— Can deal with missing data.	— No interpretability.
— Integrated OOB estimation. <sup>12</sup>	

### 4.2.5 Multivariate Adaptive Regression Splines

A Multivariate Adaptive Regression Splines (MARS) model as introduced in Friedman (1991) can be described by

$$g(x) = \sum_{m=0}^M \beta_m h_m(x),$$

where the  $h_m$  are simple functions (explained later) and the  $\beta_m$  are estimated via Least Squares. In the building procedure of a MARS model, we first select many of those simple functions and later drop some of them to avoid overfitting. For the construction of those simple functions, define  $\mathcal{B}$  the set of pairs of ‘hockey stick functions’ as:

$$\mathcal{B} := \left\{ (b_1, b_2) \mid (b_1(x), b_2(x)) = ((x_j - d)_+, (d - x_j)_+), d = X_{1,j}, \dots, X_{n,j}, j = 1, \dots, p \right\}$$

and the set  $\mathcal{M} = \{1\}$  of all functions currently in the model. Now, consider  $\mathcal{C}$  the set of candidate functions-pairs

$$\mathcal{C} := \left\{ (h(\cdot)b_1(\cdot), h(\cdot)b_2(\cdot)) : h \in \mathcal{M} \text{ and } (b_1, b_2) \in \mathcal{B} \right\} \quad (4.2.5.1)$$

and select the pair which when added to  $\mathcal{M}$  and the coefficients refitted reduces the RMSE the most. Add the selected pair to  $\mathcal{M}$  and repeat until the RMSE reduction becomes insignificant. Finally, to avoid overfitting, we prune the set  $\mathcal{M}$  by optimizing a LOOCV score.<sup>13</sup>

To reduce computational complexity, we follow the recommendation from Stephen (2021) and restrict  $h$  in equation (4.2.5.1) to be of degree one (so it is also in a pair of  $\mathcal{B}$ ). Consequently,  $\mathcal{C}$  contains functions with a degree of at most 2.

---

<sup>10</sup>That is we will sample (with replacement) several times  $n$  observations from our original data and fit a Tree to each such sample.

<sup>11</sup>Building the Tree, this time we will not test every covariate at each node (for the RMSE minimization) but a node-specific subsample of the covariates. Thus, also the ‘second best split’ can be selected.

<sup>12</sup>Estimation of  $y$  using all Trees for which  $y$  was not in the training set (cf. section 2.7.2).

<sup>13</sup>This means that we perform an iterative procedure to reduce the number of functions in  $\mathcal{M}$ . For every function  $h$  in  $\mathcal{M}$ , we compute the model using  $\mathcal{M} \setminus \{h\}$ . We discard the function that — when excluding from  $\mathcal{M}$  — leads to the best LOOCV score.

Strengths	Weaknesses
<ul style="list-style-type: none"> <li>— Catches non-linear relationships.</li> <li>— Interpretability via functions in <math>\mathcal{M}</math> and their coefficients.</li> <li>— Allows for interactions with variable selection.</li> </ul>	<ul style="list-style-type: none"> <li>— Computationally expensive (can be reduced by restricting the degree of interactions).</li> </ul>

### 4.3 Weighted Interpolation

Once we obtain the estimate  $\widehat{\text{NDVI}}^{\text{true}}$  using the models described in the previous section, we are left with the problem that not every correction is equally reliable. One such example is illustrated in figure B.4d, where the outer points (labeled as clouds) have a large scatter. Hence, we are interested in a measure of how uncertain an estimate is and thus use the absolute residuals:

$$v := \left| \text{NDVI}^{\text{true}} - \widehat{\text{NDVI}}^{\text{true}} \right| \quad (4.3.0.1)$$

Analogously as we corrected the NDVI, we replace the response  $\text{NDVI}^{\text{true}}$  with  $v$  and model its relationship with the covariates defined by  $X$ . In this way, we obtain a model for the absolute residuals  $v$  and the estimator  $\hat{v}$ . In the following, we will convert our uncertainty estimate into weights that can be used for interpolation. For this, consider a pixel, its corresponding  $\widehat{\text{NDVI}}^{\text{true}}$  and  $\hat{v}$ . In order to interpolate  $\widehat{\text{NDVI}}^{\text{true}}$ , we will give less weight to unreliable observations. Thus, we define the link function connecting  $\hat{v}$  with weights:

$$w_\tau := \frac{1}{R} \frac{1}{\hat{v}_\tau}, \quad \text{for } \tau = 1, \dots, n \quad \text{and} \quad R := \frac{1}{n} \sum_{i=1}^n \hat{v}_i \quad (4.3.0.2)$$

where  $\tau$  is an index over the satellite images and the  $R$  a normalization constant. The normalization is needed since for some IMs, inflating the sum of weights would decrease the effect of the smoothing.

### 4.4 Resulting Interpolation Strategies

We have developed the following procedure to obtain a new interpolation (keyword-wise):

- i.) LOOCV Interpolation (+ robustify?)  $\implies \text{NDVI}^{\text{true}}$
- ii.) Correction  $\implies \widehat{\text{NDVI}}^{\text{true}}$
- iii.) Uncertainty estimation  $\implies \hat{v}$  and  $w$
- iv.) Interpolation (+ robustify?)

At each step we have a choice, more precisely:

- Interpolation: SS / DL
- Robustify: Yes / No
- Correction and uncertainty estimation: RF / OLS<sup>SCL</sup> / OLS<sup>all</sup> / MARS / GAM / LASSO / no correction.

As it is not feasible to try every possible combination, we make the following restrictions on which combinations we will consider:

- We use the same IM each time.
- Either we robustify both times, or we do not robustify at all.
- We use the same underlying method for correction and uncertainty estimation.

Under those constraints on the considered combinations, we obtain 28 distinct Interpolation Strategies (ISs), which we will benchmark in the next section.

## 4.5 Evaluation via (relative) Yield Prediction Error

In this section, we introduce the (relative) Yield Prediction Error (relative YPE) and utilize it to evaluate the 28 ISs from section 4.4. The fundamental assumption is that the closer the interpolated NDVI TS is to the true one, the better it can be used to determine crop yield. Implicitly, we believe that an NDVI TS that better models yield will incorporate more true information about the underlying vegetation. Therefore, we want to determine a comparable YPE for each IS and choose it as a benchmark criterion. This is an objective measure, since we have not considered crop yield in any of our previous steps. Moreover, this criterion is justified by the fact that yield estimation has been a motivation for the interpolation.

**Definition 4.5.0.1.** (*Relative YPE*) Let  $y \in \mathbb{R}^n$  be the yield,  $M$  be a model for predicting  $y$ , and  $\hat{y} = M(X)$  where  $X$  describes the data<sup>14</sup>. Define the YPE as the RMSE in yield prediction. Formally expressed as:

$$YPE = \sqrt{\sum_{i=1}^n (y_i - \hat{y}_i)^2}.$$

Furthermore, define the relative YPE as the YPE divided by the sample mean  $\bar{y}$ .

We would like to estimate the yield from the NDVI TS produced by all the ISs for all pixels. However, given the high dimensionality and different lengths of the interpolation (not every TS has the same start and end point), we must first map each NDVI TS into a low-dimensional vector space of covariates. For this, we will use the following statistics:

- |                                   |  |
|-----------------------------------|--|
| — Maximum slope                   | — Integral <sup>15</sup> up to the peak    |
| — Minimum slope                   | — Integral <sup>15</sup> after peak        |
| — Integral <sup>15</sup> over all | — Integral <sup>15</sup> from 0-685 GDD    |
| — Peak (i.e., maximal NDVI)       | — Integral <sup>15</sup> from 685-1075 GDD |
| — GDD for the Peak                |  |

For the choice we were inspired by (cf. table 2 in Kamir et al. (2020)). However, we deliberately omit any statistic that involves the minimum (e.g., the NDVI-range), since we regard the minimum as a very error-prone measure due to the large influence of clouds in the TS. As a result, for each IS, a matrix is obtained in which each row corresponds to a pixel and both the yield and the covariates (computed by applying the above statistics) are contained. Using this matrix, we train a random forest for yield estimation, and compute

<sup>14</sup>We will use the matrixes derived in section 4.5.

<sup>15</sup>We will only consider the integral of the function  $\max(0, NDVI - 0.3)$ , where 0.3 is assumed to be a minimal NDVI value (cf. satellite images 2.3a and 2.3f with their NDVI in plot 2.3g).

the integrated OOB estimates  $\hat{y}$  (cf. section 2.7.2). Note that the choice of the modeling approach does not matter much, as long as it is general enough (i.e., able to approximate any function) and we use the same one for each IS. Finally, for each IS, we calculate the YPE and describe the results in section 5.2.

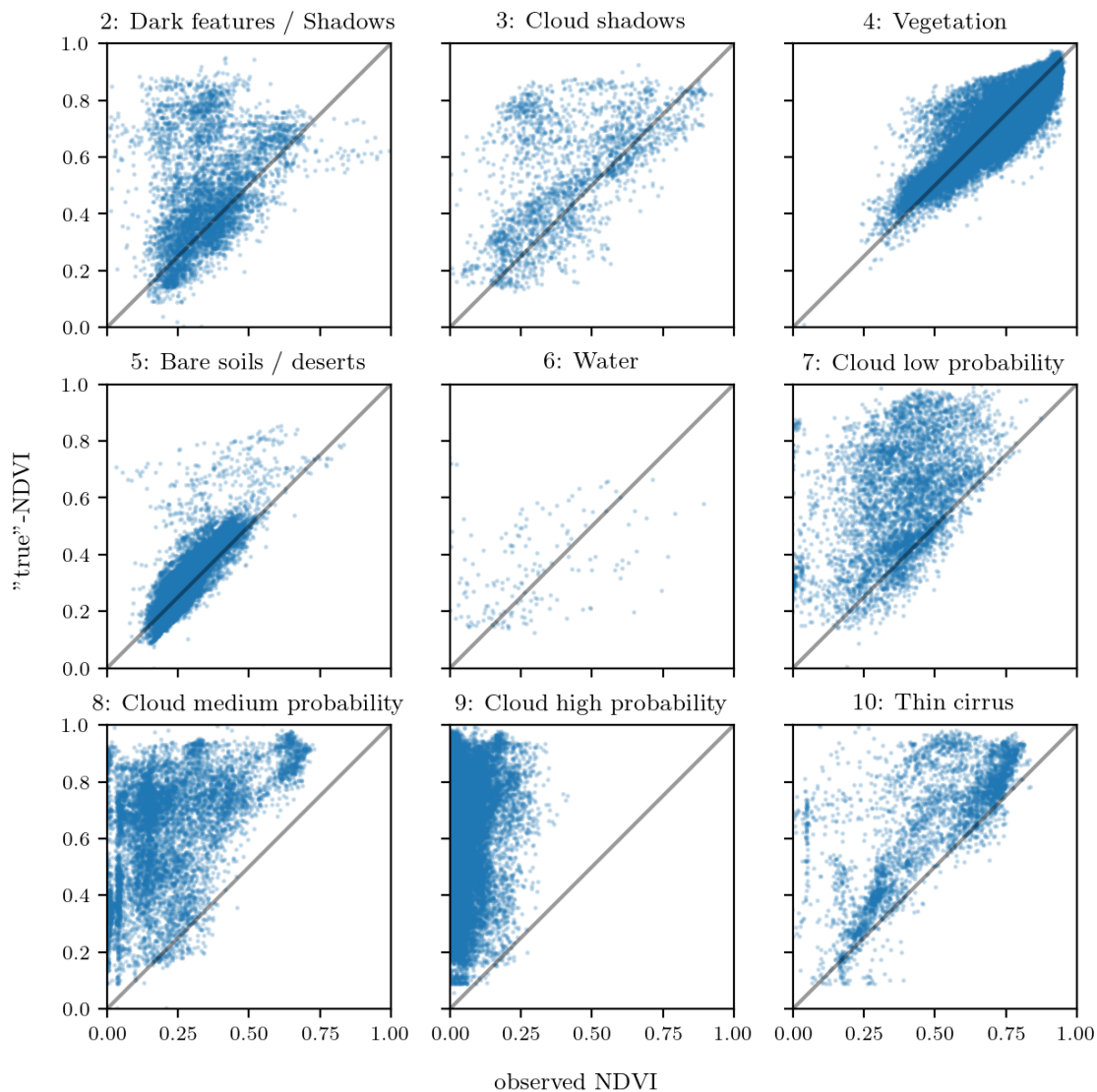


Figure 4.2: For each SCL class, we compare the true NDVI with the observed NDVI. (The true NDVI was estimated with LOOCV smoothing splines, and we used all observations of 10% of the total pixels.)



# Chapter 5

## Results

### 5.1 Goodness of Fit for Selected IMs

The benchmarks of the in section 6.1.3 selected IMs (considering only SCL45 observations) with respect to various score functions are displayed in table 5.1. The score functions summarize the absolute values of the LOOCV residuals (the smaller, the better). For each of the 5 selected IMs, we consider the basic and the robustified (see section 3.5) version.

Table 5.1: Comparing the goodness of fit for selected IMs — measured with score functions (see section 2.7.1) that take the LOOCV residuals as input. Colored row-wise.

	SS	LOESS	DL	BS	FS	SS <sup>rob</sup>	LOESS <sup>rob</sup>	DL <sup>rob</sup>	BS <sup>rob</sup>	FS <sup>rob</sup>
RMSE	0.063	0.061	0.061	0.074	0.075	0.070	0.065	0.065	0.079	0.208
QAR <sup>50</sup>	0.036	0.034	0.027	0.043	0.031	0.032	0.031	0.022	0.037	0.049
QAR <sup>75</sup>	0.063	0.061	0.051	0.077	0.058	0.061	0.057	0.044	0.070	0.099
QAR <sup>85</sup>	0.080	0.079	0.070	0.098	0.083	0.081	0.076	0.063	0.094	0.158
QAR <sup>90</sup>	0.092	0.092	0.088	0.112	0.108	0.097	0.090	0.082	0.113	0.226
QAR <sup>95</sup>	0.119	0.115	0.122	0.142	0.161	0.132	0.115	0.124	0.157	0.375

DL performs the best among both robustified and non-robustified with respect to most of the score functions used (all except QAR<sup>95</sup>) and is in particular superior to the other parametric approach, which is FS. Especially the robust FS performs poorly. The LOESS is superior than all other non-parametric methods with respect to every score function. However, it is closely followed by the SS. The BS exhibits the worst performance out of all non-parametric method tested here.

### 5.2 Yield Prediction Error for Tested ISs

The YPE for the in section 4.4 chosen ISs is given in table 5.2. We note that robustification does not improve the quality of the fit (measured via the YPE) in most cases. In terms of YPE, SS tend to be better than DL (with and without robustification), especially if no correction is made. The IS that leads to the lowest YPE is the OLS<sup>SCL</sup> with SS. Note that it is the simplest model which performs best. Given that the OLS<sup>SCL</sup> models have very good interpretability, we also present the regression equations below. The corrected

Table 5.2: Relative YPE for various ISSs. For the non-relative YPE and the coefficient of determination ( $R^2$ ) cf. table B.1 and B.2.

	RF	OLS <sup>SCL</sup>	OLS <sup>all</sup>	MARS	GAM	LASSO	no corrections
SS	0.155	0.140	0.143	0.142	0.142	0.142	0.149
SS <sup>rob</sup>	0.155	0.143	0.147	0.149	0.146	0.145	0.148
DL	0.156	0.151	0.152	0.152	0.149	0.149	0.158
DL <sup>rob</sup>	0.157	0.153	0.152	0.145	0.148	0.150	0.157

NDVI is calculated using

$$\widehat{\text{NDVI}}_{\text{true}} = 0.711 \text{NDVI}^{\text{observed}} + 0.215 \mathbb{1}_{SCL=2} + 0.237 \mathbb{1}_{SCL=3} + 0.210 \mathbb{1}_{SCL=4} \\ + 0.116 \mathbb{1}_{SCL=5} + 0.162 \mathbb{1}_{SCL=6} + 0.327 \mathbb{1}_{SCL=7} + 0.474 \mathbb{1}_{SCL=8} \quad (5.2.0.1) \\ + 0.575 \mathbb{1}_{SCL=9} + 0.306 \mathbb{1}_{SCL=10} + 0.512 \mathbb{1}_{SCL=11}$$

where  $\mathbb{1}_{SCL=2}$  is equal to one if the current observation corresponds to SCL class 2 and zero otherwise<sup>1</sup>. Whereas, we obtain the estimated absolute residuals (cf. equation 4.3.0.1) by:

$$\hat{v} = -0.133 \text{NDVI}^{\text{observed}} + 0.186 \mathbb{1}_{SCL=2} + 0.185 \mathbb{1}_{SCL=3} + 0.146 \mathbb{1}_{SCL=4} \\ + 0.089 \mathbb{1}_{SCL=5} + 0.167 \mathbb{1}_{SCL=6} + 0.203 \mathbb{1}_{SCL=7} + 0.181 \mathbb{1}_{SCL=8} \quad (5.2.0.2) \\ + 0.173 \mathbb{1}_{SCL=9} + 0.180 \mathbb{1}_{SCL=10} + 0.172 \mathbb{1}_{SCL=11}$$

Thus, if we observe a pixel with SCL class 4 ('vegetation') but a NDVI of only 0.4, the corrected NDVI would be  $0.711 \cdot 0.4 + 0.21 = 0.494$  with an estimated absolute residual of  $-0.133 \cdot 0.4 + 0.146 = 0.093$ . In equation 5.2.0.1, we notice the strongest upwards correction for SCL classes 8, 9 and 11 ('medium probability clouds', 'high probability clouds' and 'thin cirrus clouds'). The estimated absolute residuals, however, are the smallest for SCL classes 4 and 5 ('vegetation' and 'bare soil'). Furthermore, the higher the observed NDVI the lower are the estimated absolute residuals. For the R-output of the `summary` function of the two models, we refer to the appendix B.3.1.

<sup>1</sup> $\mathbb{1}$  is also called an indicator function or characteristic function in mathematics.

# Chapter 6

## Discussion

In the first part of the discussion, we argue the choice of the score function, examine IMs for compatibility with data gaps and argue choices for selected IMs. In the second part, we argue against using meteorological data, identify the best IS and address issues in yield estimation.

### 6.1 Interpolation

#### 6.1.1 Score Functions

In situ data is generally preferred for evaluating IMs. Being difficult to obtain, [Li et al. \(2021\)](#) generated NDVI TS by introducing random noise to an idealized NDVI curve that has been constructed by considering many pixeles and taking the pointwise mean of their NDVI TS. Because the distribution of the noise is chosen by the authors, they do not have to deal with systematic outliers and adequately, given the circumstances, use the non-robust RMSE. On the other hand, the generated NDVI TS no longer contain the typical challenges (underestimated NDVI and data gaps). Thus, the authors test their IMs more for general interpolation reliability, and less for challenging S2-derived NDVI TS. To adequately test our IMs for those challenges, we employ the LOOCV.

[Cai et al. \(2017b\)](#) evaluate various IMs based solely on the RMSE. We see the choice of the RMSE for the selection of the IMs as problematic, because it is sensitive to outliers. Yet we know that systematic outliers are present in our data (cf. figure 2.3d). Thus, when we consider the RMSE as a score function, we do not choose the IM that disregards outliers, but is heavily influenced by them. Likewise, [Liemohn et al. \(2021\)](#) confirms that the RMSE, in the presence of outliers, is not sufficient. [Barron \(2019\)](#) proposes a robust score function, a more flexible variant of the Huber loss function ([Huber, 1964](#)). For simplicity's sake, we choose the robust QAR<sup>x</sup> score function (cf. definition 2.7.1.2). For example, QAR<sup>90</sup> can easily handle up to 10% of outliers (i.e., contaminated data points) in the data.

#### 6.1.2 Data Gaps in Time Series

NW estimates the value for the time  $t$  by relating to the points near  $t$ . To determine what ‘near’ means, a bandwidth  $h$  is used (cf. equation 3.3.1.2). This approach becomes infeasible as soon as the data gaps become larger than  $h$ , since no points are left that are

close to  $t$ . Using a locally adaptive bandwidth fix (Brockmann et al., 1993), we pay with a greater variability of the estimator. According to the authors, a small sample size (as we have it for the NDVI TS) worsens this situation. For GK, we expect, due to the stationarity assumption, that in regions with no data the interpolation will tend to the mean (cf. figure 3.3). The SG cannot handle data gaps since it requires equidistant data points. Chen et al. (2004) proposes a linear interpolation to restore missing data points. However, due to the non-linear timescale transformation to GDD in section 2.4, the requirement of equidistant remains an unresolved issue. The FS interpolation can be corrupted if there are noticeable data gaps, as can be observed in figure 3.1. Additionally, the poor goodness-of-fit values for the robustified variant in table 5.1 illustrate the unreliability of this IM method. The robustified values in table 5.1 are meaningful in describing the ability to cope with data gaps, since more data points are ignored during the robustification and hence data gaps are simulated. Similarly, for SS, LOESS, DL, and BS we compare the values in table 5.1 between the robustified and non-robust variant. Unlike as for FS, the robust variant does not differ significantly from the non-robust variant. Thus, we conclude that these methods do not exhibit systematic failures frequently. Regarding the LOESS, the weights can attain non-intuitive values in case of data gaps. The result can be a strongly fluctuating behavior, as observed in figure 3.6 in plot (c). There, a strange peak between the first and second observation is visible. This peak originates from local weighting. In estimating the peak value, the first data point in the plot, although adjacent to the peak, is given a low weight compared to the points to the right of the peak. Due to strong shape assumptions, DL handles data gaps well. However, it may happen that the model describes the NDVI increase as abrupt. This, however, was fixed by bounding the first derivative (cf. section 3.2.3).

### 6.1.3 Preselection

Here we justify our preselection of the IMs tested in section 3.6. We decided against NW because of its systematic errors at peaks and valleys and poor handling of data gaps (cf. section 6.1.2). UK will not be considered since the underlying stationarity assumption is not met and therefore a systematic bias is introduced. On top of that, maximum likelihood parameter estimation might lead to overfitting (cf. figure 3.3). Also, we do not include SG, since we see LOESS as a more favourable generalization. The remaining IMs are thus SS, LOESS, DL, BS, and FS.

### 6.1.4 Candidate Selection

At this point we choose which IMs will be considered in chapter 4. Given that DL convinces, regarding most of the selected score functions in table 5.1, we will further consider this IM. Furthermore, we see that in most cases the robustification improved the score regarding QAR<sup>50</sup>, QAR<sup>75</sup>, QAR<sup>85</sup> and QAR<sup>90</sup>. Only for the outlier-sensitive score functions (RMSE and QAR<sup>95</sup>)<sup>1</sup> we notice significant worsening (we consider the robust FS separately in section 6.1.2). Consequently, we will also apply the robustification in chapter 4. In order to not only rely on the shape assumptions of the DL, we additionally choose a flexible non-parametric IM for further consideration. Despite the LOESS slightly dominating the SS in table 5.1, we choose the SS. We justify this selection with the non-smooth behavior of the LOESS in case of data gaps (see section 6.1.2) and the good interpretability of the

<sup>1</sup>For the RMSE one outlier is enough to take away the usefulness of the statics, in the case of QAR<sup>95</sup> it is enough if 5% of the data are contaminated to break the statics.

SS from minimizing function 3.3.6.1.

## 6.2 NDVI Correction

### 6.2.1 Using Additional Covariates

In section 4.2 we have only used covariates derived from spectral data. We decided against using meteorological data, since we consider five years of data not to be sufficient to model patterns of how vegetation reacts to various weather events. Moreover, we expect the weather in our study region to be rather homogeneous, which is suggested by the fact that the meteorological data published by Meteoswiss are for a grid with a resolution of 1 km. On the other hand, we want the underlying model not to learn improper relationships. For example, the model might automatically predict a high NDVI for a day in summer (detected by high GDD or many sunshine hours) just because it is ‘used’ to observing a lot of vegetation in summer. Including temporally (e.g.,  $P_{t-1}$  and  $P_{t+1}$ ) and geographically adjacent pixels would likely improve performance. However, for simplicity, we omitted it here<sup>2</sup>.

### 6.2.2 IS Selection

The evaluation of various ISs via the YPE in section 5.2 shows that SS are better suited than DL for yield estimation. Moreover, it seems surprising that robustification tends to worsen the results, despite reducing LOOCV residuals in most cases (cf. section 5.1). We conjecture that the correction models handle outliers by themselves (by correcting or down-weighting them) and thus do not benefit from an external robustification. Indeed, for OLS<sup>SCL</sup> we see in equation 5.2.0.2 that the smaller the observed NDVI of a point, the larger the estimated residual — yielding a lower weight. This coincides with our experience that outliers usually underestimate the NDVI. Our conjecture is consistent with the fact that if we do not correct, robustification produces a marginal improvement.

If we use the best IS without correction ( $SS^{rob}$ ) the relative RMSE of the NDVI-based yield prediction is 0.148 (cf. table 5.2). Using the best IS with correction ( $SS+OLS^{SCL}$ ), instead results in a relative RMSE of 0.140. Later, in section 6.2.3, we explain why those results might be too optimistic but argue that they are still valid for relative comparison. Hence, we compare the amount of unexplained variance of the NDVI-based yield prediction. When correcting with  $SS+OLS^{SCL}$  instead of only using  $SS^{rob}$ , the unexplained variance decreases by

$$\frac{0.148^2 - 0.140^2}{0.148^2} = 10.5\%.^3$$

Note that the results discussed here depend strongly on the link function used (cf. equation 4.3.0.2). Once we change it, we should also repeat this analysis.

### 6.2.3 Error Sources in Yield Estimation

Although the YPE was not our primary goal, but was only used as a means to select the best IS, we compare our values with the corresponding ones by Perich et al. (2022).

---

<sup>2</sup>This is done for simplicity of understanding and using the model, since one would need to adapt to some convention of how to supply the data of adjacent pixels without redundancy (i.e., supplying  $P_t$  multiple times). Another complication would be a border-pixel with some adjacent pixels outside the field.

<sup>3</sup>The same result may be obtained via the  $R^2$  values from appendix table B.2:  $\frac{(1-0.705)-(1-0.736)}{1-0.705} = 10.5\%$

There, a YPE 1.00 [t/ha] was obtained using meteorological data in addition to NDVI TS. Since our error is only about 3.3% larger (cf. table B.1), we consider our results to be competitive. Especially as we did not use meteorological data aside from the timescale transformation (cf. section 2.4), and in contrary did not scale the yield down by 10% (cf. section 2.2). In the following, we ask ourselves how much modelling performance we can expect. This will be limited by multiple sources of uncertainty in the data:

- i.) Uncertainty in yield data collected by the combine harvester (Robinson and Metternicht, 2005).
- ii.) Uncertainty in yield data through rasterization.
- iii.) Contamination of satellite images through clouds and other atmospheric effects (cf. section 2.6).
- iv.) Heterogeneity within one pixel might lead to a less informative NDVI value.<sup>4</sup>
- v.) Uncertainty introduced by interpolating NDVI TS, especially when long data-gaps are present.

Even if we had a perfect NDVI curve, it contains only a fraction of the information about the underlying vegetation. Nonetheless, Perich et al. (2022) manages to explain up to 86% of the variance in crop yield with only the NDVI TS and meteorological data (Table 5). Although the authors divided the data into training and test data, this subdivision was done randomly at pixel level (without subdividing into fields or years). Thus, there are pixels in the training data that are neighboring pixels from the test data and consequently exhibit high correlations (in yield and spectral reflectances). We suspect that these high values are due to overfitting via high-correlation pixels. This line of argument is consistent with the poor results in table 6 for cross-year-validation — i.e., each year represents a single fold. The authors, however, account them to uneven (extreme) weather. If this is not rather caused by the suspected overfitting, could be investigated by performing a cross-field-validation — i.e., cross-year-validation with splitting each year further into the respective fields. Since we have multiple fields per year, during evaluation each model trained will have seen the weather of all years but no adjacent pixels. Nevertheless, we claim, that our results are not affected by spatial correlation of neighboring pixels. This is because our result is not a 'good' YPE, but the selected IS. Furthermore, we expect all tested ISs to benefit equally from this correlation in terms of YPE, and we are only interested in the relative differences.

#### 6.2.4 NDVI Correction as Unsupervised Learning

The question arises, if we can build the correction model on the same year as we want to apply it on. Usually, a similar approach might carry the danger of overfitting. However, we have not used any ground truth at any point (until the evaluation). Instead, we estimated the 'true' NDVI with the assumption 4.1.0.1 via OOB. Hence, we developed an unsupervised learner of the NDVI. The degree of overfitting can be objectively assessed with the YPE. Using the IS corresponding to the best YPE, we do not expect strong overfitting. Consequently, we reason that our method can be applied to a new comparable dataset.

---

<sup>4</sup>For example, if one pixel is covered densely with vegetation on one half while the other half is covered with dry soil, the mean reflectancy does not correspond to the mean vegetation density. This is caused by the fast saturation of the NDVI (Gu et al., 2013).

# Chapter 7

## Conclusion

In this thesis, we investigated how to model vegetation dynamics through NDVI TS derived from satellite images. The major challenges were how to deal with contaminated observations (due to clouds or shadows) and how to interpolate the observed NDVI values. A summary of the IMs considered can be found in the table 3.

Filtering the observations contaminated by clouds and shadows via SCL introduces data gaps, especially in winter. Therefore, we aim for IMs that handle such data gaps well. The Nadaraya-Watson kernel estimator struggles when there are no or too few points in the window of interest; Universal Kriging is biased towards the mean, particularly in environments with no data (cf. figure 3.3); 2<sup>nd</sup> order Fourier series can deviate strongly within data gaps (cf. figure 3.1) and the Savitzky-Golay filter depends on equidistant observations (cf. section 6.1.2). Occasionally, a generalization of the Savitzky-Golay filter — the Locally Weighted Regression — has also shown surprising behavior in data gaps (cf. figure 3.6).

In contrast, the latter performed well in Leave-One-Out-Cross-Validation (LOOCV) (cf. table 5.1). Nevertheless, we prefer the Smoothing Splines (SS) as they perform only slightly worse there, but produce a much smoother curve (cf. figure 3.5 and 3.6). SS flexibly approximate the data while keeping curvature low (cf. equation 3.3.6.1). B-splines, on the other hand, were worse than SS with respect to every score function tested, and their smoothing mechanism is also less interpretable. However, the best performing method here is the approximation by a Double logistic (DL), which makes strong assumptions about the shape of the NDVI curve. Problems for the parameter estimation of the DL (and the FS) have been resolved by restricting the parameter space by generous but realistic values. Problems with overfitting in universal kriging were overcome by determining the variogram parameters for a subsample of NDVI TS and finally using the median of each parameter. In the end, we choose DL and SS as our preferred IMs.

The traditional answer to the question of how to deal with contaminated observations is that we only consider observations that are labeled as vegetation or bare soil by the SCL (SCL45). The unreliability of this labeling, however, is illustrated in figure 2.3. Moreover, filtered observations (non-SCL45) might still contain valuable information (see section 4.1). Therefore, we do not adhere to traditional (SCL) filtration, but instead consider all observations and correct the observed NDVI with uncertainty estimations. For this, we use statistical models that take additional information such as the remaining spectral bands, the current SCL label and the observed NDVI into account. But before we interpolate

the corrected NDVI values, we assign a weight to each observation, corresponding to its uncertainty. The uncertainty is estimated analogously as the NDVI has been corrected. That is, taking the same covariates but replacing the old response ( $\text{NDVI}^{\text{true}}$ ) with a new one ( $\text{abs}(\text{NDVI}^{\text{corrected}} - \text{NDVI}^{\text{true}})$ ). By combining different IMs with various statistical models, we obtain 28 different Interpolation Strategies (ISs) (see section 4.4). To assess which of these ISs is best, we assume that the better the IS, the better it allows interpolated NDVI TS to predict yield. Surprisingly, the best strategy is the one with SS and the simplest static model considered, which uses only the observed NDVI and SCL classification. Let us recapitulate the best IS: First, we estimate the ‘true’ NDVI (c.f. assumption 4.1.0.1) using SS via LOOCV. Then obtain the corrected NDVI using the  $\text{OLS}^{\text{SCL}}$  model (cf. equation 5.2.0.1). Subsequently, we estimate the absolute error with the  $\text{OLS}^{\text{SCL}}$  model (cf. equation 5.2.0.1) and thereby obtain weights which are supposed to reflect the reliability of the corrected NDVI (cf. equation 4.3.0.2). Finally, we perform a weighted interpolation with SS.

To make the IMs more robust to contaminated observations (outliers) that remained after SCL filtration, we generalized an iterative technique. After an initial fit, in each iteration we give less weight to observations with comparatively large residuals and then perform a weighted interpolation (see section 3.5). However, after too many iterations, non-contaminated points might get ignored (i.e., given a zero weight). The greatest improvements, on the other hand, were perceived after the first iteration (see figure 3.5). For evaluating the generalized robustification technique, we used raw LOOCV performance on the one hand, and the ability to model the NDVI TS for crop yield estimation on the other hand. On the one hand, robustification (narrowly) misses the target of being part of the best IS. On the other hand, we see in table 5.1 that robustification leads to smaller LOOCV residuals in most cases. That is (except for the Fourier approximation) the  $\text{QAR}^{50}$  and  $\text{QAR}^{75}$  are smaller for the robustified ones. Hence, when we expect contaminated observations, we advise to robustify the interpolation.

As to the question of which IM we recommend, we consider two cases. If one only intends to fit a curve to the NDVI TS as precisely as possible, we recommend the robustified DL, since it minimizes the LOOCV residuals in most cases (cf. table 5.1). In the event that one requires an interpolation that contains as much information about the plant as possible, we recommend SS. This recommendation is especially valid if we traditionally consider only SCL45 observations without correcting the proposed NDVI. However, we recommend the abovementioned IS with NDVI correction, because it reduces the unexplained variance of the NDVI-based yield prediction by 10.5% (cf. section 6.2.2). Considering all the error sources (cf. section 6.2.3) and the fact that we only consider the NDVI TS, we consider the 10.5% to be a solid improvement.

## 7.1 Future Work

### 7.1.1 Time Series Correction-Interpolation as a General Method

Throughout this thesis, we developed a correcting uncertainty-weighted interpolation procedure for the NDVI. However, we never relied on any properties of the NDVI. Only the parameter estimated via cross-validation in chapter 3.4 depends on the scale of the TS. For simplicity, we could thus determine the parameter using Generalized Cross Validation (Ripley and Maechler, 2022). Therefore, our approach of interpolation and correction of TS can be applied to arbitrary TS if additional information is available. This includes TS

outside of satellite imagery or remote sensing. However, further research is required, to demonstrate the general usefulness of this approach.

As an example, we could perform cloud-correction with uncertainty estimation and interpolation. In the same manner as we corrected the NDVI TS for a pixel in chapter 4, one could look at each spectral band separately and correct it with an uncertainty estimate. Subsequently, one reassembles the corrected bands and translates the multiple estimated uncertainties into one. Optionally, the TS can also be interpolated before merging, as in chapter 4.3. The remaining question is how such an approach might perform.

### 7.1.2 Minor Improvements

During this project, we also noticed some minor issues that we would have liked to investigate further if more resources had been available. The most relevant of these are:

- **Data:** The method how the combine harvester point cloud has been extrapolated to the 10m grid of S2 could possibly be improved.
- **Data:** We have not included the spectral bands that have a resolution of 60 m. But precisely these seem to be promising for cloud correction, since they are a proxy of the water (content and form) in the atmosphere.
- **Data:** [Raiyani et al. \(2021\)](#) present a machine learning approach that supposedly improves the SCL and thus could improve our results that are based on the SCL.
- **NDVI Correction:** Explore the effect of different link and normalizing functions in section 4.3. Currently, we run into the danger of some outer points getting nearly ignored because one estimated absolute residual for some interior point is close to zero.
- **NDVI Correction:** Yield is not the only target variable of interest. Other variables like protein content could also be used in section 4.5 for the method evaluation.



# Bibliography

- Atzberger, C. and P. H. Eilers (2011, September). A time series for monitoring vegetation activity and phenology at 10-daily time steps covering large parts of South America. *International Journal of Digital Earth* 4(5), 365–386.
- Barron, J. T. (2019, April). A General and Adaptive Robust Loss Function.
- Beck, P. S. A., C. Atzberger, K. A. Høgda, B. Johansen, and A. K. Skidmore (2006, February). Improved monitoring of vegetation dynamics at very high latitudes: A new method using MODIS NDVI. *Remote Sensing of Environment* 100(3), 321–334.
- Breiman, L. (2001, October). Random Forests. *Machine Learning* 45(1), 5–32.
- Brockmann, M., T. Gasser, and E. Herrmann (1993, December). Locally Adaptive Bandwidth Choice for Kernel Regression Estimators. *Journal of the American Statistical Association* 88(424), 1302–1309.
- Bühlman, P. and M. Maechler (2020, October). Computational Statistics.
- Cai, Z., P. Jönsson, H. Jin, and L. Eklundh (2017a, December). Performance of Smoothing Methods for Reconstructing NDVI Time-Series and Estimating Vegetation Phenology from MODIS Data. *Remote Sensing* 9(12), 1271.
- Cai, Z., P. Jönsson, H. Jin, and L. Eklundh (2017b, December). Performance of Smoothing Methods for Reconstructing NDVI Time-Series and Estimating Vegetation Phenology from MODIS Data. *Remote Sensing* 9(12), 1271.
- Cao, R., Y. Chen, M. Shen, J. Chen, J. Zhou, C. Wang, and W. Yang (2018, November). A simple method to improve the quality of NDVI time-series data by integrating spatiotemporal information with the Savitzky-Golay filter. *Remote Sensing of Environment* 217, 244–257.
- Chandola, V. and R. R. Vatsavai (2010). Scalable time series change detection for biomass monitoring using Gaussian Processes. *Conference on Intelligent Data Understanding*, 14.
- Chen, J., P. Jönsson, M. Tamura, Z. Gu, B. Matsushita, and L. Eklundh (2004, June). A simple method for reconstructing a high-quality NDVI time-series data set based on the Savitzky–Golay filter. *Remote Sensing of Environment* 91(3), 332–344.
- Cleveland, W. S. (1979, December). Robust Locally Weighted Regression and Smoothing Scatterplots. *Journal of the American Statistical Association* 74(368), 829–836.
- Courault, D., L. Hossard, V. Demarez, H. Dechatre, K. Irfan, N. Baghdadi, F. Flamain, and F. Ruget (2021, July). STICS crop model and Sentinel-2 images for monitoring rice

- growth and yield in the Camargue region. *Agronomy for Sustainable Development* 41(4), 49.
- Craven, P. and G. Wahba (1978, December). Smoothing noisy data with spline functions. *Numerische Mathematik* 31(4), 377–403.
- Diggle, P. J. and P. J. Ribeiro (2007). Gaussian models for geostatistical data. In *Model-Based Geostatistics*, pp. 46–78. New York, NY: Springer.
- Eilers, P. H. C. (2003, July). A Perfect Smoother. *Analytical Chemistry* 75(14), 3631–3636.
- ESA (2022a, August). European Space Agency: Level-2A Algorithm Overview. <https://sentinels.copernicus.eu/web/sentinel/technical-guides/sentinel-2-msi/level-2a/algorithms>.
- ESA (2022b, August). Sentinel-2. <https://sentinel.esa.int/web/sentinel/missions/sentinel-2>.
- Friedman, J. H. (1991, March). Multivariate Adaptive Regression Splines. *The Annals of Statistics* 19(1), 1–67.
- Gamon, J. A., C. B. Field, M. L. Goulden, K. L. Griffin, A. E. Hartley, G. Joel, J. Penuelas, and R. Valentini (1995). Relationships Between NDVI, Canopy Structure, and Photosynthesis in Three Californian Vegetation Types. *Ecological Applications* 5(1), 28–41.
- Gu, Y., B. K. Wylie, D. M. Howard, K. P. Phuyal, and L. Ji (2013, July). NDVI saturation adjustment: A new approach for improving cropland performance estimates in the Greater Platte River Basin, USA. *Ecological Indicators* 30, 1–6.
- Gurung, R. B., F. J. Breidt, A. Dutin, and S. M. Ogle (2009, October). Predicting Enhanced Vegetation Index (EVI) curves for ecosystem modeling applications. *Remote Sensing of Environment* 113(10), 2186–2193.
- Hastie, T. and R. Tibshirani (1987, June). Generalized Additive Models: Some Applications. *Journal of the American Statistical Association* 82(398), 371–386.
- Henits, L., Á. Szerletics, D. Szokol, G. Szlovák, E. Gojdár, and A. Zlinszky (2022, January). Sentinel-2 Enables Nationwide Monitoring of Single Area Payment Scheme and Greening Agricultural Subsidies in Hungary. *Remote Sensing* 14(16), 3917.
- Holzkämper, A., D. Fossati, J. Hiltbrunner, and J. Fuhrer (2015, January). Spatial and temporal trends in agro-climatic limitations to production potentials for grain maize and winter wheat in Switzerland. *Regional Environmental Change* 15(1), 109–122.
- Huber, P. J. (1964). Robust Estimation of a Location Parameter. *The Annals of Mathematical Statistics* 35(1), 73–101.
- Jaramaz, D., V. Perović, S. Belanovic Simic, E. Saljnikov, D. Cakmak, V. Mrvić, and L. Zivotic (2013, May). The ESA Sentinel-2 mission Vegetation variables for Remote sensing of Plant monitoring.
- Kamir, E., F. Waldner, and Z. Hochman (2020, February). Estimating wheat yields in Australia using climate records, satellite image time series and machine learning methods. *ISPRS Journal of Photogrammetry and Remote Sensing* 160, 124–135.

- Li, S., L. Xu, Y. Jing, H. Yin, X. Li, and X. Guan (2021, December). High-quality vegetation index product generation: A review of NDVI time series reconstruction techniques. *International Journal of Applied Earth Observation and Geoinformation* 105, 102640.
- Liemohn, M. W., A. D. Shane, A. R. Azari, A. K. Petersen, B. M. Swiger, and A. Mukhopadhyay (2021, July). RMSE is not enough: Guidelines to robust data-model comparisons for magnetospheric physics. *Journal of Atmospheric and Solar-Terrestrial Physics* 218, 105624.
- Lyche, T. and K. Morken (2005, January). Spline Methods.
- McMaster, G. S. and W. W. Wilhelm (1997, December). Growing degree-days: One equation, two interpretations. *Agricultural and Forest Meteorology* 87(4), 291–300.
- Miller, P., W. Lanier, and S. Brandt (2018, July). Using Growing Degree Days to Predict Plant Stages.
- Omori, K., T. Sakai, J. Miyamoto, A. Itou, A. N. Oo, and A. Hirano (2021, April). Assessment of paddy fields' damage caused by Cyclone Nargis using MODIS time-series images (2004–2013). *Paddy and Water Environment* 19(2), 271–281.
- Perich, G., H. Aasen, J. Verrelst, F. Argento, A. Walter, and F. Liebisch (2021, January). Crop Nitrogen Retrieval Methods for Simulated Sentinel-2 Data Using In-Field Spectrometer Data. *Remote Sensing* 13(12), 2404.
- Perich, G., M. O. Turkoglu, L. V. Graf, J. D. Wegner, H. Aasen, A. Walter, and F. Liebisch (2022, July). Pixel-based crop yield mapping and prediction using spectral indices and neural networks on Sentinel-2 time series data.
- Raiyani, K., T. Gonçalves, L. Rato, P. Salgueiro, and J. R. Marques da Silva (2021, January). Sentinel-2 Image Scene Classification: A Comparison between Sen2Cor and a Machine Learning Approach. *Remote Sensing* 13(2), 300.
- Ripley, B. D. and M. Maechler (2022, August). R: Fit a Smoothing Spline. <https://stat.ethz.ch/R-manual/R-patched/library/stats/html/smooth.spline.html>.
- Robinson, T. P. and G. Metternicht (2005, July). Comparing the performance of techniques to improve the quality of yield maps. *Agricultural Systems* 85(1), 19–41.
- Rouse, J. W. (1974, May). Monitoring the vernal advancement and retrogradation (green wave effect) of natural vegetation. Technical Report NASA-CR-139243.
- Savitzky, A. and M. J. E. Golay (1964, July). Smoothing and Differentiation of Data by Simplified Least Squares Procedures. *Analytical Chemistry* 36(8), 1627–1639.
- Schafer, R. W. (2011, July). What Is a Savitzky-Golay Filter? [Lecture Notes]. *IEEE Signal Processing Magazine* 28(4), 111–117.
- Stephen, M. (2021, July). Earth: Multivariate Adaptive Regression Splines.
- Stöckli, R. and P. L. Vidale (2004, September). European plant phenology and climate as seen in a 20-year AVHRR land-surface parameter dataset. *International Journal of Remote Sensing* 25(17), 3303–3330.
- Strbac, O., M. Milanovic, and V. Ogrizovic (2017, July). Estimation the evapotraspiration of urban parks with field based and remotely sensed datasets. pp. 13.

- Tibshirani, R. (2011). Regression shrinkage and selection via the lasso: A retrospective. *Journal of the Royal Statistical Society: Series B (Statistical Methodology)* 73(3), 273–282.
- Verhoeven, G. and L. Jo (2006, December). Looking through Black-Tinted Glasses – A Remotely Controlled Infrared Eye in the Sky.

# Appendix A

## Reproducibility

### A.1 Reproduce Results

For reproducibility of the whole computations, we refer to our codebase at:

<https://github.com/LGraz/MasterThesis-Code>

In order to reproduce our computations and results, set up the directory as described in the README. The ‘Yield Mapping’ Data used, is published alongside Perich et al. (2022). Execute the computations via the script `./shell_scripts/reproduce.sh` and do not execute the python and R files by hand (unless you follow the order in `./shell_scripts/reproduce.sh`).

### A.2 R-Package

We also provide an R package for a general time series correction and interpolation if additional data is available at:

<https://github.com/LGraz/CorrectTimeSeries>

In our case, we consider the NDVI time series and the additional data consists of the unused spectral bands.

We recommend installing it via the `devtools` package by:

```
devtools::install_github("LGraz/CorrectTimeSeries")
```

In the following, we shall give a stand-alone example of how the R package can be used:

```
1 library(CorrectTimeSeries)
2 data(timeseries_list) # load NDVI-TS data
3
4 # Add "true" NDVI (or generally the response), by Out-Of-Bag estimation
5 timeseries_list <- lapply(timeseries_list, function(df) {
6   df$oob_ndvi <- OOB_est(df$gdd, df$ndvi_observed) # gdd is the time-axis
7   df
8 })
9
10 # Train correction model
11 formula <- "oob_ndvi ~ B02+B03+B04+B05+B06+B07+B08+B8A+B11+B12+scl_class"
12 RF <- train_RF_with_formula(formula, timeseries_list, robustify = TRUE)
13
14 # ADD CORRECTION
15 timeseries_list <- lapply(timeseries_list, function(df) {
16   df$corrected_ndvi <- randomForest:::predict.randomForest(RF, df)
17   df
18 })
19
```

```
20 # Get interpolation for each timeseries
21 lapply(timeseries_list, function(df) {
22   ss ← smoothing_spline(df$gdd, df$corrected_ndvi)
23   predict(ss, 1:1000)$y
24 })
```

Example of how to use the **CorrectTimeSeries** package

## Appendix B

# Further Material

### B.1 Data and Methods

#### B.1.1 NDVI

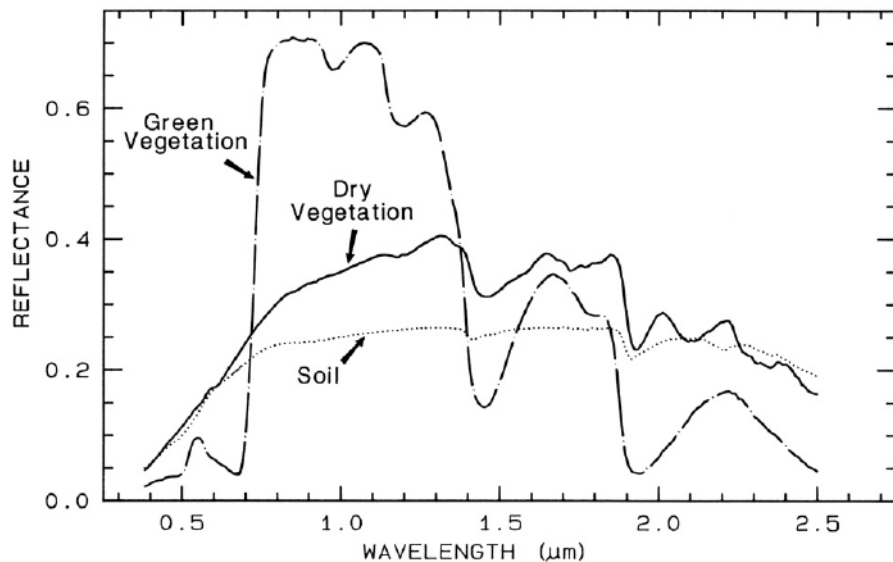


Figure B.1: Spectral reflectance of the green/dry vegetation compared with soil. Note the strong jump at  $0.7\mu\text{m}$  which is utilized in the NDVI. Figure taken from [Verhoeven and Jo \(2006\)](#)

#### B.1.2 GDD

[Miller et al. \(2018\)](#) tabulates the corresponding GDD for each stage of wheat.

Stage	Description	GDD
Emergence	Leaf tip just emerging from above-ground coleoptyle.	125 – 160
Leaf development	Two leaves unfolded.	169 – 208
Tillering	First tiller visible	369 – 421
Stem elongation	First node detectable.	592 – 659
Anthesis	Flowering commences; first anthers of cereals are visible.	807 – 901
Seed fill	Seed fill begins. Caryopsis of cereals watery ripe (first grains have reached half of their final size).	1068 – 1174
Dough stage	Soft dough stage, grain contents soft but dry, fingernail impression does not hold.	1434 – 1556
Maturity complete	Grain is fully mature and drydown begins. Ready for harvest when dry.	1538 – 1665

## B.2 Interpolation

### B.2.1 Parameter Bounds

As discussed in section 3.2.3 we encountered parameter optimization issues which we solved via bounding them.

For the DL (cf. section 3.2.1) we assumed:  $y_{min} \in [0, 0.7]$ ,  $y_{max} \in [0.4, 1]$ ,  $t_0 \in [100, 1500]$ ,  $t_1 \in [800, 3000]$ ,  $d_0 \in [0, 0.01]$  and  $d_1 \in [-0.01, 0]$ .

For the FS (cf. section 3.2.2) we assumed:  $T \in [1200, 4000]$ ,  $a_0 \in [-1, 2]$ ,  $a_1 \in [-5, 5]$ ,  $a_2 \in [-5, 5]$ ,  $b_1 \in [-5, 5]$  and  $b_2 \in [-5, 5]$ .

### B.2.2 Iterations for Robustification

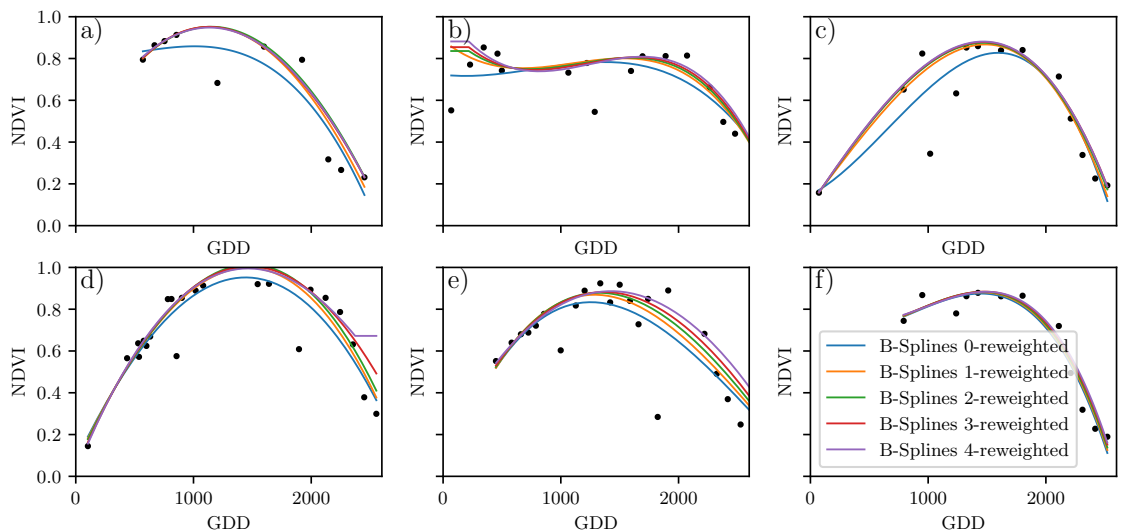


Figure B.2: B-splines fitted to different (SCL45) NDVI TS. Iterations of a robustifying refit (as indicated in section 3.5) are also displayed.

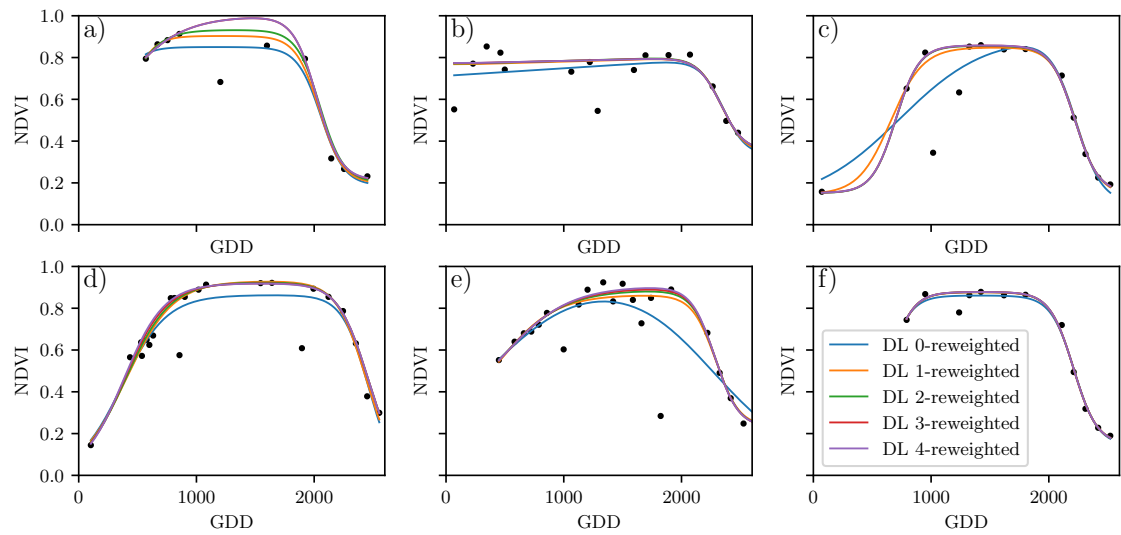


Figure B.3: A Double Logistic curve fitted to different (SCL45) NDVI TS. Iterations of a robustifying refit (as indicated in section 3.5) are also displayed.

### B.3 NDVI correction

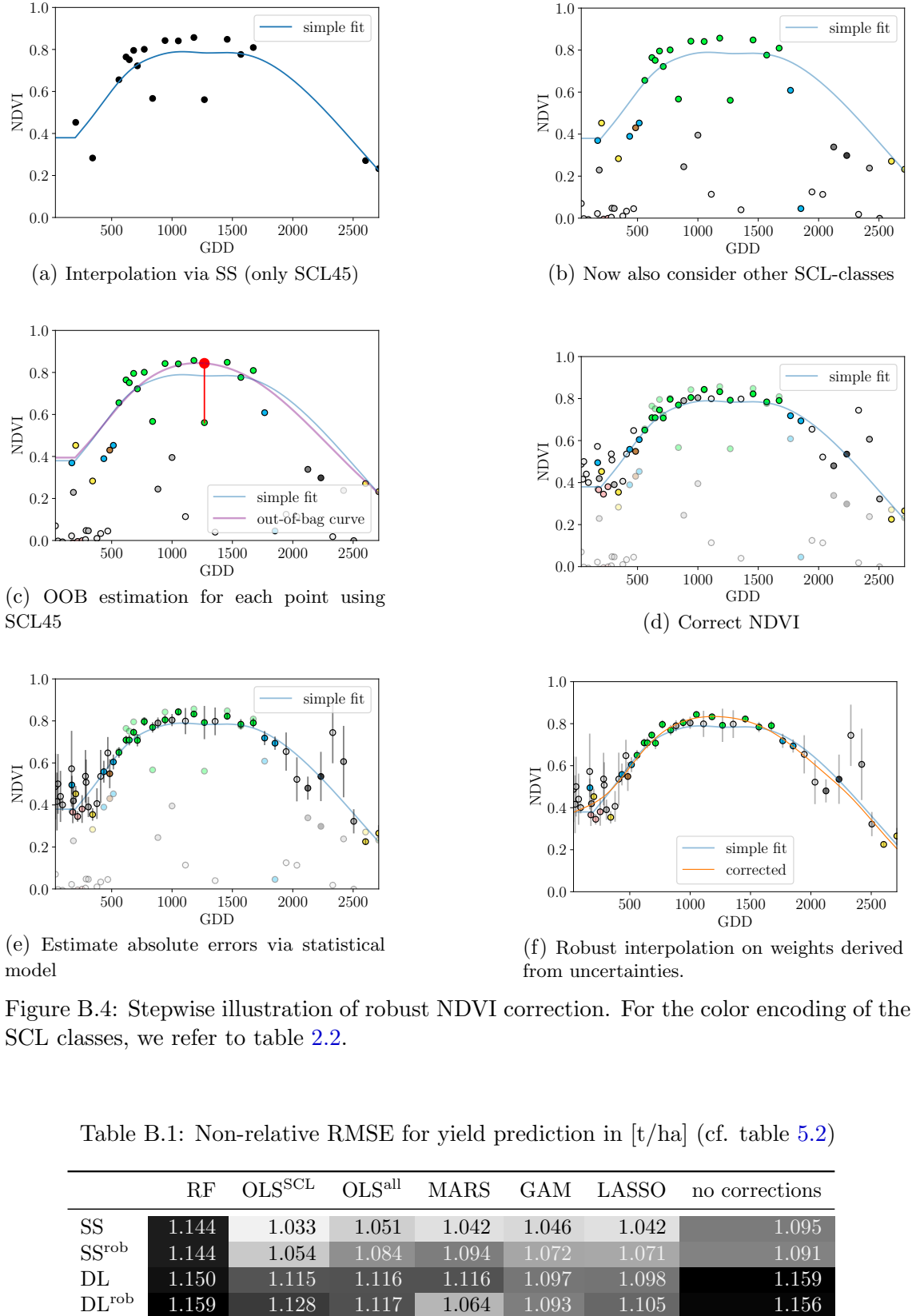


Figure B.4: Stepwise illustration of robust NDVI correction. For the color encoding of the SCL classes, we refer to table 2.2.

Table B.1: Non-relative RMSE for yield prediction in [t/ha] (cf. table 5.2)

	RF	OLS <sup>SCL</sup>	OLS <sup>all</sup>	MARS	GAM	LASSO	no corrections
SS	1.144	1.033	1.051	1.042	1.046	1.042	1.095
SS <sup>rob</sup>	1.144	1.054	1.084	1.094	1.072	1.071	1.091
DL	1.150	1.115	1.116	1.116	1.097	1.098	1.159
DL <sup>rob</sup>	1.159	1.128	1.117	1.064	1.093	1.105	1.156

Table B.2: Coefficient of determination ( $R^2$ ) of yield prediction (cf. table 5.2)

	RF	OLS <sup>SCL</sup>	OLS <sup>all</sup>	MARS	GAM	LASSO	no correction
SS	0.676	0.736	0.726	0.731	0.729	0.731	0.703
SS <sup>rob</sup>	0.676	0.724	0.709	0.704	0.715	0.716	0.705
DL	0.672	0.692	0.691	0.691	0.702	0.701	0.667
DL <sup>rob</sup>	0.667	0.685	0.690	0.719	0.704	0.697	0.669

### B.3.1 OLS<sup>SCL</sup> Model Outputs

```

1 Call:
2 lm(formula = (paste(response, " ~ ", "ndvi_observed + scl_class")),
3     data = ndvi_df)
4
5 Residuals:
6   Min     1Q Median     3Q    Max
7 -0.7997 -0.0717  0.0039  0.0695  0.6632
8
9 Coefficients:
10                      Estimate Std. Error t value Pr(>|t|)
11 (Intercept)          0.21465  0.00230   93.46 < 2e-16 ***
12 ndvi_observed        0.71116  0.00346  205.65 < 2e-16 ***
13 scl_class3           0.02205  0.00356    6.20  5.8e-10 ***
14 scl_class4          -0.00431  0.00251   -1.72   0.085 .
15 scl_class5          -0.09875  0.00234  -42.15 < 2e-16 ***
16 scl_class6          -0.05301  0.01104   -4.80  1.6e-06 ***
17 scl_class7           0.11245  0.00274   41.09 < 2e-16 ***
18 scl_class8           0.25963  0.00253  102.57 < 2e-16 ***
19 scl_class9           0.35994  0.00236  152.47 < 2e-16 ***
20 scl_class10          0.09091  0.00308   29.54 < 2e-16 ***
21 scl_class11          0.29784  0.00392   76.06 < 2e-16 ***
22 ---
23 Signif. codes:  0 '***' 0.001 '**' 0.01 '*' 0.05 '.' 0.1 ' ' 1
24
25 Residual standard error: 0.146 on 124978 degrees of freedom
26 Multiple R-squared:  0.532,      Adjusted R-squared:  0.532
27 F-statistic: 1.42e+04 on 10 and 124978 DF,  p-value: <2e-16

```

R Summary of the NDVI correction model (cf. equation 5.2.0.1)

```

1 Call:
2 lm(formula = (paste(get_res(), " ~ ", "ndvi_observed + scl_class")),
3     data = ndvi_df)
4
5 Residuals:
6   Min     1Q Median     3Q    Max
7 -0.2051 -0.0427 -0.0074  0.0329  0.6589
8
9 Coefficients:
10                      Estimate Std. Error t value Pr(>|t|)
11 (Intercept)          0.18647  0.00126  147.74 < 2e-16 ***
12 ndvi_observed       -0.13265  0.00190  -69.80 < 2e-16 ***
13 scl_class3           -0.00180  0.00196   -0.92  0.3587
14 scl_class4          -0.04069  0.00138  -29.55 < 2e-16 ***
15 scl_class5          -0.09698  0.00129  -75.32 < 2e-16 ***
16 scl_class6          -0.01906  0.00606   -3.14  0.0017 **
17 scl_class7           0.01641  0.00150   10.91 < 2e-16 ***
18 scl_class8          -0.00560  0.00139   -4.02  5.7e-05 ***
19 scl_class9          -0.01384  0.00130  -10.67 < 2e-16 ***
20 scl_class10          0.00690  0.00169   -4.08  4.5e-05 ***
21 scl_class11          0.01446  0.00215   -6.72  1.8e-11 ***
22 ---
23 Signif. codes:  0 '***' 0.001 '**' 0.01 '*' 0.05 '.' 0.1 ' ' 1
24
25 Residual standard error: 0.08 on 124978 degrees of freedom

```

```
26 | Multiple R-squared:  0.352,      Adjusted R-squared:  0.352  
27 | F-statistic: 6.8e+03 on 10 and 124978 DF,  p-value: <2e-16
```

R Summary of the NDVI correction model (cf. equation 5.2.0.2)

# Declaration of Originality

The signed declaration of originality is a component of every semester paper, Bachelor's thesis, Master's thesis and any other degree paper undertaken during the course of studies, including the respective electronic versions.

Lecturers may also require a declaration of originality for other written papers compiled for their courses.

---

I hereby confirm that I am the sole author of the written work here enclosed and that I have compiled it in my own words. Parts excepted are corrections of form and content by the supervisor .

**Title of work** (in block letters):

INTERPOLATION AND CORRECTION OF  
MULTISPECTRAL SATELLITE IMAGE TIME SERIES

**Authored by** (in block letters):

*For papers written by groups the names of all authors are required.*

Name(s):

GRAZ

First name(s):

LUKAS

With my signature I confirm that

- I have committed none of the forms of plagiarism described in the Citation etiquette information sheet.
- I have documented all methods, data and processes truthfully.
- I have not manipulated any data.
- I have mentioned all persons who were significant facilitators of the work .
- I am aware that the work may be screened electronically for plagiarism.
- I have understood and followed the guidelines in the document *Scientific Works in Mathematics*.

Place, date:

18. 09.2022 Zürich

Signature(s):

Graz

*For papers written by groups the names of all authors are required. Their signatures collectively guarantee the entire content of the written paper.*